Elsevier Editorial System(tm) for Nuclear Inst. and Methods in Physics Research, A
Manuscript Draft

Manuscript Number: NIMA-D-20-00032R1

Title: Natural background radiation at Lab 2 of Callio Lab, Pyhäsalmi mine in Finland

Article Type: Full length article

Section/Category: Space Radiation and Underground Detectors

Keywords: Environmental radioactivity; Gamma spectrometry; Neutron flux; Deep underground laboratory; Uranium concentration; Radioactivity content

Corresponding Author: Dr. Kinga Polaczek-Grelik, Ph.D.

Corresponding Author's Institution: University of Silesia

First Author: Kinga Polaczek-Grelik, Ph.D.

Order of Authors: Kinga Polaczek-Grelik, Ph.D.; Agata Walencik-Łata, PhD; Katarzyna Szkliniarz, PhD; Jan Kisiel, prof.; Karol Jędrzejczak, PhD; Jacek Szabelski, PhD; Marcin Kasztelan, PhD; Jerzy Orzechowski; Przemysław Tokarski; Włodzimierz Marszał; Marika Przybylak; Jari Joutsenvaara; Hannah J Puputti; Marko Holma; Timo Enqvist, PhD

Abstract: In operating mines, as well as in deep locations for planned scientific activities, it is essential to recognize the natural background radiation from the point of view of both occupational hazard and experimental background. Callio Lab, located in the Pyhäsalmi Mine, Finland, is one of the underground laboratories participating in the Baltic Sea Underground Innovation Network (BSUIN). The characterization of the natural background radiation was done at the Lab 2, which is the deepest located in Callio Lab. It involved in-situ gamma spectrometry, thermal neutron flux measurements, radon concentration determination, and α/β laboratory spectrometry of water and rock samples. At a depth of 1436 m (~4000 m w.e.) within the felsic volcanic bedrock occurs a volcanogenic massive sulphide deposit, wherein a thermal neutron flux of (1.73 ± 0.10)×10^-5 cm^-2s^-1, a gamma-ray flux of 12.7 ± 1.5 cm^-2s^-1, a gamma-ray dose of 0.158 ± 0.029 μSv/h and a radon concentration of 213.3 Bq/m^3 ± 11% were determined.

Chorzów, January,14, 2020

To the Editor of the *Nuclear Instruments and Methods in Physics Research Section A: Accelerators, Spectrometers, Detectors and Associated Equipment*
Peter Krizan

DearProf. Krizan,

On behalf of the BSUIN project group, I would like to submit to the Nuclear Instruments and Methods in Physics Research Section A paper:
” Natural background radiation at Lab 2 of Callio Lab, Pyhäsalmi mine in Finland”.

This paper is the report about the natural radiation in shallow underground site and contains the in situ measurements of neutrons and gamma radiation, and laboratory investigations of uranium and radium content in rock and water samples. It is aimed at characterization of the deep underground laboratory as potential site for physics, technology, biology and material science experiments. The work has been carried out within the Baltic Sea Underground Innovation Network (BSUIN) project supported by the EU’s Interreg Baltic Sea Region Programmeand and it is the second report of our group as a continuation of research that were published in NIM A last year.

Sincerely yours,

KingaPolaczek-Grelik, PhD

Natural background radiation at Lab 2 of Callio Lab, Pyhäsalmi mine in Finland

Kinga Polaczek-Grelik[a,b*], Agata Walencik-Łata[a], Katarzyna Szkliniarz[a], Jan Kisiel[a], Karol Jędrzejczak[c], Jacek Szabelski[c], Marcin Kasztelan[c], Jerzy Orzechowski[c], Przemysław Tokarski[c], Włodzimierz Marszał[c], Marika Przybylak[c], Jari Joutsenvaara[d], Hannah J. Puputti[d], Marko Holma[d,e,f], Timo Enqvist[d]

[a] University of Silesia in Katowice, August Chełkowski Institute of Physics, 75 Pulku Piechoty 1, 41-500 Chorzow, Poland
kinga.grelik@gmail.com, *corresponding author
agata.walencik@us.edu.pl
katarzyna.szkliniarz@us.edu.pl
jan.kisiel@us.edu.pl
[b] NU-Med Cancer Diagnosis and Treatment Centre Katowice, Ceglana 35, 40-514 Katowice, Poland
[c] National Centre for Nuclear Research, 28 Pulku Strzelcow Kaniowskich 69, 90-001 Lodz, Poland
kj@zpk.u.lodz.pl
js@zpk.u.lodz.pl
mk@zpk.u.lodz.pl
jo@zpk.u.lodz.pl
tokarski@zpk.u.lodz.pl
wm@zpk.u.lodz.pl
mp@zpk.u.lodz.pl
[d] University of Oulu, Kerttu Saalasti Institute Pajatie 5, 85500 Nivala, Finland
jari.joutsenvaara@oulu.fi
hannah.puputti@oulu.fi
marko.holma@gmail.com
timo.t.enqvist@gmail.com
[e] Muon Solutions Oy, Rakkarinne 9, 96900 Saarenkylä, Finland
marko.holma@muon-solutions.com
[f] Arctic Planetary Science Institute, Lihtaajantie 1 E 27, FI-44150 Äänekoski, Finland

Conflicts of Interest: The authors declare no conflicts of interest.

Abstract

In operating mines, as well as in deep locations for planned scientific activities, it is essential to recognize the natural background radiation from the point of view of both occupational hazard and experimental background. Callio Lab, located in the Pyhäsalmi Mine, Finland, is one of the underground laboratories participating in the Baltic Sea Underground Innovation Network (BSUIN). The characterization of the natural background radiation was done at the Lab 2, which is the deepest located in Callio Lab. It involved in-situ gamma spectrometry, thermal neutron flux measurements, radon concentration determination, and α/β laboratory spectrometry of water and rock samples. At a depth of 1436 m (~4000 m w.e.) within the felsic volcanic bedrock occurs a volcanogenic massive sulphide deposit, wherein a thermal neutron flux of $(1.73 \pm 0.10)\times10^{-5}$ $cm^{-2}s^{-1}$, a gamma-ray flux of

12.7 ± 1.5 $cm^{-2}s^{-1}$, a gamma-ray dose of 0.158 ± 0.029 μSv/h and a radon concentration of 213.3 Bq/m^3 ± 11% were determined.

Keywords: environmental radioactivity, gamma spectrometry, neutron flux, deep underground laboratory, uranium concentration, radioactivity content

1. Introduction

Nowadays, the Underground Laboratories (ULs) offer more and more possibilities not only for physical, biological and environmental sciences but also for industrial test benches, business and agriculture [1-6]. They ensure a low radioactive background environment which is essential to perform the physics experiments searching for rare phenomena, and required for research in other areas. The depth and the level of natural radioactivity are two main parameters characterizing ULs. Both have a direct influence on the sensitivity of measurements. Therefore, the precise determination of natural radioactivity is essential. Complete characterization of the natural background radiation in an UL includes the estimation of the concentration of natural radioisotopes in rock and water, concentration of radon in air, and measurements of neutron and muon fluxes. The known main sources of background radiation are: cosmic ray (including muon) interactions, the decays of primordial radionuclides (mainly ^{40}K, ^{232}Th, and ^{238}U), the neutron interactions that originate from (α,n) reactions, the spontaneous fission of U and Th. The contribution from gaseous Rn coming from alpha decays of ^{226}Ra originating from the rock has to be taken into account as well. ULs are shielded with rock overburden which decreases the number of high energy neutrons created by cosmic-ray muon interactions [7]. These components influence radioactive hazard inside the underground halls. Therefore careful investigations of in-situ gamma radioactivity and neutron flux, supplemented by the laboratory analysis of rock and water samples give the complete characterization of radiation environment in an UL.

This paper presents the results of in-situ gamma spectrometry, in-air radon concentration determination and neutron flux measurements performed at a depth of 1436 m (4000 m w.e.) in Callio Lab, Pyhäsalmi, Finland. The results of the laboratory analysis of the uranium and radium content in the rock and water samples, collected therein, are also included. The muon flux measurements have not been performed, since the muon component was fully characterised earlier [8]. The paper is organized as follows: after a description of the site, a characterization of the applied experimental methods is provided. It is followed by the results, including a detailed analysis of the gamma radioactivity, neutron flux measurements, and uranium concentrations in the rock and water samples. Discussion and conclusions section finishes the paper.

1.1 Site geology

The Pyhäsalmi mine is located in the Vihanti-Pyhäsalmi belt in the northeastern part of the Paleoproterozoic Svecofennian domain of the Fennoscandian shield. The Vihanti-Pyhäsalmi belt contains two large volcanogenic massive sulphide (VMS) deposits, from which the Pyhäsalmi deposit is the larger (75.7 Mt). The deposit was formed originally as a by-product of a submarine synvolcanic hydrothermal system. The Pyhäsalmi VMS deposit forms an elongated accumulation of base metal sulphides stretching from the current erosional level down to 1400 m depth. The deposit has a flat, subvertical shape and it can be subdivided into two ore bodies separated from each other by a shear zone: the upper ore body is 1000 m long, 150-650 m wide and 10-60 m thick and extends from the surface to about 1000 m depth, whereas the deep ore forms a 300-400 m wide and 200-300 m thick "potato"-shaped sulphide body between about 1000 m and 1400 m depths. Regarding valuable metals, the ore contain on average 0.92% Cu, 2.45% Zn, 37.4% S, 0.4 g/t Au and 14 g/t Ag [9]. The ore is characterised by massive pyrite and subordinate amounts of sphalerite, chalcopyrite, pyrrhotite, dolomite, calcite and baryte. There also occur minor amounts of arsenopyrite, bournonite, electrum, galena, gold, hessite, jordanite, magnetite, marcasite, molybdenite, seligmannite and tetrahedrite.

A major proportion of the ore occurs within the domain of hydrothermally altered Rhyolite B unit that extends to more than 1 km depth [9]. The altered rock types are mainly in the form of sericite schist and cordierite-anthophyllite rock. The present metamorphic mineral assemblages of this rock type are dominated by muscovite, cordierite, quartz, biotite and baryte. Radioactive minerals are not part of the alteration or metamorphic mineral assemblages or at least are exceedingly rare. Other wall rocks of the ore include mica schist, felsic tuff, tholeiitic basalt, dolomitic marble and late unaltered mafic dykes. In addition, there occur voluminous pink, red and light grey pegmatite dykes near the eastern tectonised contact of the deposit, especially alongside the deep ore. Drill hole data from depths greater than 1400 m indicate that the bedrock underneath the deep ore is dominated by a mafic volcanic rock with interlayers of felsic volcanic rocks, pegmatite, tonalite and skarn [10]. Table 1 summarises the mineralogical compositions and typical density ranges of the main rock types in the Pyhäsalmi mine.

Table 1. An overview of the mineral components in the region of Pyhäsalmi mine. Only the most important accessory minerals are included. Most densities are taken from [11].

Rock/formation	Main mineral content	Formula
Felsic volcanic rocks (rhyolites) ~2.72 g/cm³ (all), ~2.71 g/cm³ (unaltered), ~2.76 g/cm³ (altered, no sulphides), ~ 2.84 g/cm³ (altered, with sulphides), ~2.92 g/cm³ (altered sericite-quartz schist)	Quartz	SiO_2
	Muscovite	$KAl_2(AlSi_3O_{10})(F,OH)_2$
	Biotite	$K(Mg,Fe)_3(AlSi_3O_{10})(F,OH)_2$
	Feldspar (albite plagioclase)	$Na(AlSi_3O_8)$
	Cordierite	$(Mg,Fe)_2Al_4Si_5O_{18}$
	Sillimanite	Al_2SiO_5
	Hornblende (in unaltered varieties)	$(Ca,Na)_{2-3}(Mg,Fe,Al)_5(Al,Si)_8O_{22}(OH,F)_2$
	+ occasionally some sulphides	

Mafic volcanic rocks (basalts) ~2.92 g/cm³ (all), ~2.94 g/cm³ (unaltered), ~ 2.85 g/cm³ (altered, no sulphides), ~ 3.14 g/cm³ (altered, with sulphides)	Orthoamphibole (anthophyllite)	$(Mg,Fe)_2(Mg,Fe)_5Si_8O_{22}(OH)_2$
	Biotite	$K(Mg,Fe)_3(AlSi_3O_{10})(F,OH)_2$
	Cordierite	$(Mg,Fe)_2Al_4Si_5O_{18}$
	Garnet	$X_3Z_2(SiO_4)3$, wherein X = Mg, Ca, Fe(II), Mn(II), etc., and Z = Al, Fe(III), Cr(III), V(III), etc.
	Sillimanite	Al_2SiO_5
	Plagioclase	$Ca(Al_2Si_2O_8)$
	Quartz	SiO_2
	+ occasionally some sulphides	
Pegmatite ~2.68 g/cm³	Potassium feldspar	$KAlSi_3O_8$
	Quartz	SiO_2
Sulphide ore (VMS) ~3.49 to 4.55 g/cm³	Pyrite (most voluminous main mineral)	FeS_2
	Sphalerite (main mineral)	ZnS
	Chalcopyrite (main mineral)	$CuFeS_2$
	Pyrrhotite (main mineral)	$Fe_{1-x}S$, wherein x = 0 to 0.17
	Dolomite (main mineral)	$CaMg(CO_3)_2$
	Calcite (main mineral)	$CaCO_3$
	Sericite	$KAl_2(AlSi_3O_{10})(OH)_2$
	Baryte (main mineral)	$BaSO_4$
	Arsenopyrite (accessory mineral)	FeAsS
	Bournonite (accessory mineral)	$PbCuSbS_3$
	Galena (accessory mineral)	PbS
	Magnetite (accessory mineral)	Fe_3O_4
	Molybdenite (accessory mineral)	MoS_2

From various rock types in Pyhäsalmi, rhyolites, felsic tuffs and pegmatite dykes are most likely the primary sources of radioactivity in the mine, although it is worth noting that also skarns may contribute. From these rock types, pegmatite dykes are way more likely to contain radioactive minerals than the other three rock types. These assessments are based on common geochemical fractionation and other typical geological processes that favour enrichment of radioactive elements to such rock types while depressing their enrichment in the other rock types in the area. To the best of our knowledge, the only radioactive minerals occurring in the mine are zircon ($ZrSiO_4$) and titanite ($CaTiSiO_5$). Zircons are commonly slightly radioactive due to the trace amounts of U and Th, whereas uranium concentration in titanite is usually rather high, between 100 and 1000 ppm. However, due to the lack of detailed mineralogical investigations on pegmatites, one cannot be sure that zircon and titanite are the only radioactive minerals in Pyhäsalmi. It is also possible that some parts of some of the pegmatite dykes contain greater amounts of radioactive minerals than so far documented (e.g. in small few centimetre wide pockets).

Among the elements constituting minerals in the Pyhäsalmi region, characterised in Table 1, Al, Fe, Na, Mn, Zn, Cu, Sb and Mo have isotopes with (n,γ) reaction cross-section above 0.1 b [12].

This means that the activation of neutron-excess radioisotopes could appear even in the presence of a moderate neutron flux and high contribution of the thermal component of this flux will enhance this process. From the above-mentioned elements, Na, Mn and Al have only one stable nuclide, therefore it is quite easy to observe the activation in these cases. Elements like Fe, Zn, and Mo have stable consecutive isotopes, which means the neutron capture on these elements does not result in the production of a radionuclide. The products of neutron activation are mostly β^-radioactive; however, annihilation photons might also occur, since ^{65}Zn, ^{64}Cu and ^{122}Sb are positron emitters. The energies of decay gamma rays, for which ^{28}Al, ^{59}Fe, ^{24}Na, ^{56}Mn, ^{65}Zn, ^{64,66}Cu, ^{122,124}Sb and ^{99,101}Mo activated radionuclides are the sources, cover the range from 81 keV (^{101}Mo) to 2754 keV (^{24}Na) [12]. The main admixtures found in the rock types from the Pyhäsalmi mine are Ag, Au, As, Bi, Ni, Co. Among them, activation of ^{198}Au and ^{60}Co is the most common, which is followed by the emission of decay gamma rays of 412 keV and 1173+1332 keV, respectively [12].

Callio Lab, Finland, consists of four underground research facilities, Lab 1-4, presented in Fig. 1. The facilities vary from old tunnels refurbished for re-use activities to tunnels constructed specially for the research. The measurements for this report were conducted in Lab 2 of Callio Lab. It is located at a depth of 1436 m in the Pyhäsalmi Mine, and it consists of two halls, an entrance hall (~700 m^3) – Hall 1, and an experimental hall of 120 m^2 (~1000 m^3) – Hall 2 (see Fig. 1 and 2a). The air to the experimental hall is blown from the elevator shaft through ventilation pipes with an air influx of 10 m^3/s prior to the air filtration unit. This is done for the supply of fresh air and also for mitigating the radon level. The background radiation measurements were conducted at several measuring points (MPs), and samples were collected from several drillholes or equivalent locations both inside and adjacent to the aforementioned halls and outside the entrance hall.

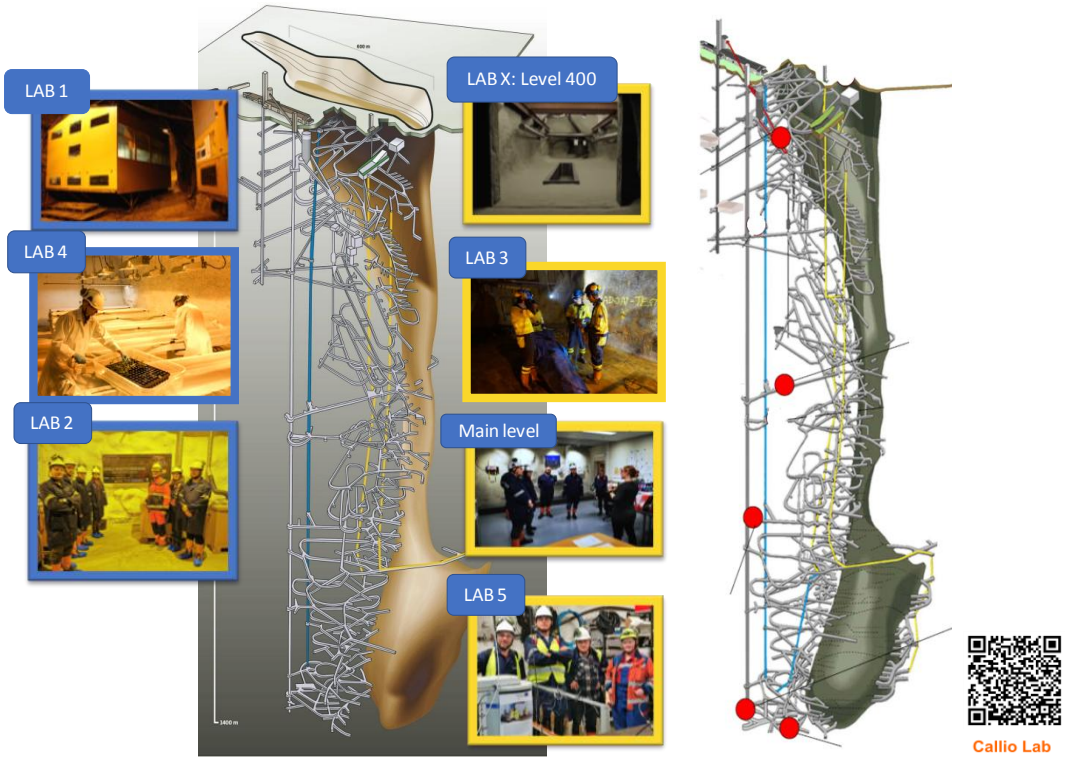

Figure 1. Pyhäsalmi mine layout with the locations of the laboratories and QR code to the SketchUp of the 3D model. Lab 1 – 75 m below the ground, Lab 2 – 1436 m, Lab 3 – 990 m and Lab 4 – 660 m, Lab 5 – 1410 m, Lab X – 400 m, Main level office – intelligent lighting pilot. More details could be found at: calliolab.com

From the geological point of view, both of the halls of Lab 2 are located within a body of rock dominated by mafic volcanic rocks and subordinate pegmatite and felsic volcanic rocks [13]. The walls have been covered with 5-10 cm thickness of shotcrete, a fast-drying sprayable concrete to ensure rock stability together with rock bolts. The used shotcrete contains up to 30 % of furnace slag, a waste material of the iron industry. Depending on the source and patch the furnace slag concentrations for ^{40}K, ^{226}Ra and ^{232}Th are up to 140 ± 11 Bq/kg, 160 ± 32 Bq/kg, 240 ± 19 Bq/kg, respectively [14], as determined by the laboratory of Finnish Nuclear Safety Authority.

2. Equipment and Methods

The main measuring location was chosen near the far right corner of the experimental hall (Hall 2, MP 1 in Fig. 2) in Lab 2. The Hall 2 cavern (9 m high, 15 m long and 8 m wide) drilled in the granite bedrock with a volcanic sulphide deposit is coated with a layer of shotcrete. An in-situ gamma-ray high-purity germanium (HPGe) semiconductor spectrometer, a RAD7 electronic radon detector (Durridge Company, Inc.), a neutron helium proportional counters were used. Additionally, rock and water samples collected in and outside the Lab 2 were analysed using liquid scintillation α/β counting (LSC), alpha and gamma spectrometry techniques. 48-hour in-situ gamma spectrometry and 45-hour neutron flux measurements were performed in the MP1 Hall 2 in Lab 2. The samples of rock, concrete from the wall and water gathered from the boreholes exiting the were collected for the laboratory

analysis. Additionally, two more measurement locations (MP 2 and MP 3 in Fig. 2) have been selected at the central points of Hall 2 and Hall 1. In each measuring point (MP1 – MP3), the registration of the gamma-ray spectrum was accompanied by the 24-h measurement of in-air radon concentration. This procedure allows the recognizing of the sources of radon origin (ventilation ducts and the emanation from the rock as the product of radium decay) and contribution of each of them. A water sample and radon measurement were also acquired from the location outside the entrance to Lab 2 (see: Fig. 2f) for comparison purposes.

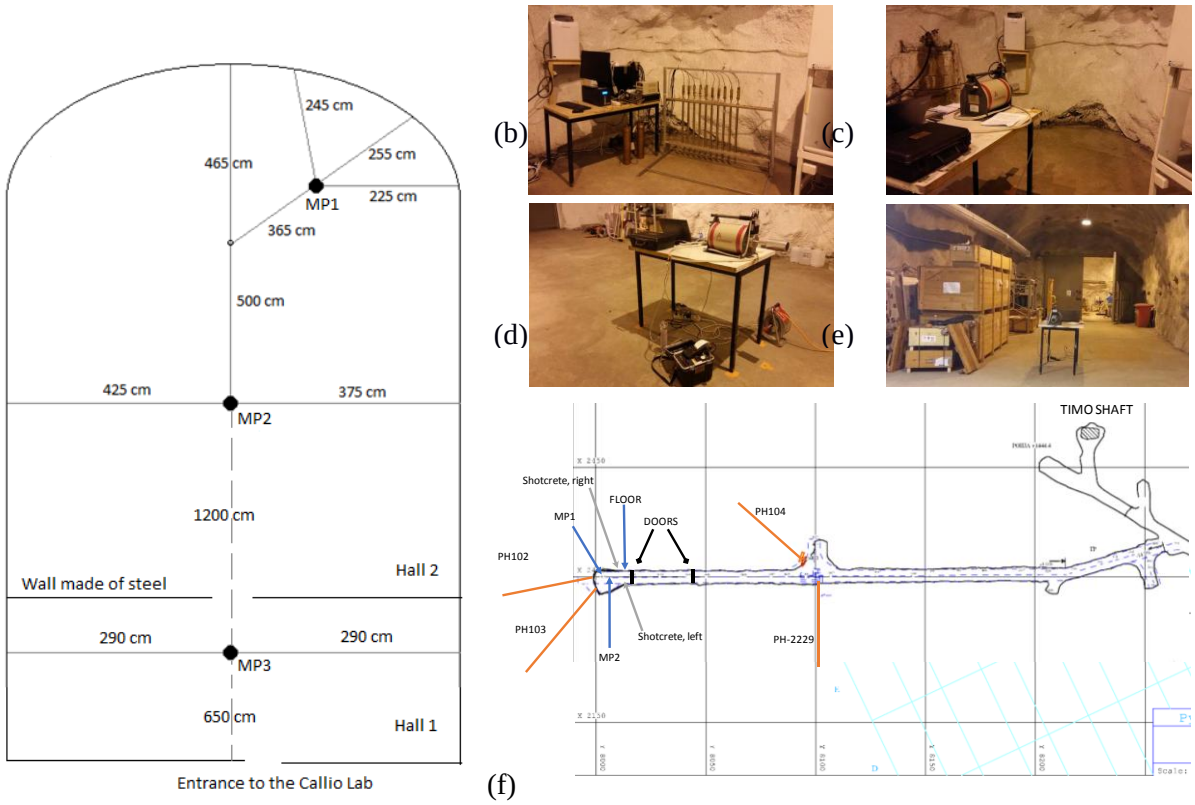

Figure 2. Experimental setup: (a) the scheme of Lab 2 (not in scale) with measuring points (MPs) and pictures of detectors' positions: (b) helium counters between the wall and MP1, (c) HPGe spectrometer in MP1, (d) HPGe spectrometer and RAD7 monitor in MP2, (e) HPGe spectrometer in MP3 positioned in Hall 1 (entrance hall shown in Fig. 1), (f) the layout of Level 1436 m in Pyhäsalmi mine.

2.1 In-situ gamma spectrometry

Equipment for in-situ gamma spectrometry measurements consisted of:

- liquid nitrogen cooled semiconductor HPGe detector GR4020-7935-7F-RDC-4 (Canberra Industries, Inc.) having: 40% nominal efficiency, 0.6 mm carbon composite entrance window, resolution of 2.1 keV FWHM at 1.33 MeV ^{60}Co line and the peak-to-Compton ratio of 57/1,
- InSpector 2000^{TM} multichannel (8194 channels) analyzer (Canberra Industries, Inc.),
- Genie^{TM} 2000 v.3.2.1 acquisition and analysis software (Canberra Industries, Inc.).

The measuring range of this detector covers energies from about 7 keV to 3.15 MeV when applying a total spectrometric gain of 5.0. The HPGe detector was oriented horizontally and placed 1 m above the

concrete-coated floor on a table, as presented in Fig. 2. Energy calibration (covering the range of 14 – 2506 keV) was performed using a set of sealed radioactive sources (1 cm in diameter and about 10 kBq activity): ^{133}Ba, ^{137}Cs, ^{54}Mn, ^{57}Co, ^{109}Cd, ^{22}Na and ^{60}Co. Identification of in-situ registered radioisotopes was based on the photopeaks' energies. Radioisotopes recognized on registered spectra subsequently underwent quantitative analysis using detection efficiency calibration performed with the use of a geometry of *room/box with internal surface contamination*, modelled in Geometry Composer software (Canberra Industries, Inc.), applying ISOCS™ software (Canberra Industries, Inc.) and monoenergetic photons covering the energy range of 10 – 3300 keV (an adequate measuring range). Subsequently, the calibration functions were fitted to each geometry (1. inside Hall 2 and 2. inside Hall 1) in the form of 5th order polynomial

$$\ln(\varepsilon) = a + b\cdot\ln(E) + c\cdot\ln(E)^2 + d\cdot\ln(E)^3 + e\cdot\ln(E)^4 + f\cdot\ln(E)^5. \quad (1)$$

The positioning of the detector, as well as the dimensions of each hall, were taken into account.

Monoenergetic photon flux density was calculated from the photopeak areas employing detection efficiency curve ε(E), taking into account Ge crystal surface area (S_{Ge}) and lifetime of spectrum acquisition (LT):

$$\Phi(E)\ \left[cm^{-2}s^{-1}\right] = \frac{Peak\_net\_area(E)}{\varepsilon(E)\cdot S_{Ge}\left[cm^2\right]\cdot LT[s]}. \quad (2)$$

The uncertainty assessment was based on 10% average uncertainty of efficiency value (given in Genie 2000™ software) and photopeak area uncertainty obtained during the procedure of automatic peak searching and fitting, performed in Genie 2000™ software, using an unidentified second differential and non-linear least-squares fit. These two main sources of final photon flux density error have been treated as independent from each other.

Subsequently, apparent radioactivity at a point of measurement (A [Bq/cm^2]) of each radionuclide recognized on the registered spectra was calculated taking into account photon flux density, obtained previously, and quantum efficiency of emission of photons with a given energy during radioactive decay (taken from Tables of Isotopes [12]). The final activity of each radioisotope was calculated as an average over activities obtained on the base of a single flux density of monoenergetic photons (given photopeak area on the spectrum). The discrepancy between elemental results obtained in such a way has been expressed as the standard deviation of the mean value.

The effective dose rate at each point of measurements was assessed on the base of monoenergetic photon flux density (calculated previously), using conversion coefficients for ISO geometry taken from [15]. The conversion coefficients for exact energies of registered photons were obtained using Lagrange interpolation formula of 3rd degree (4-point), on the base of the values given therein for discrete monoenergetic photons from the range 0.01 – 10 000 MeV. The results were subsequently grouped according to the radioisotopes emitting monoenergetic photons under study. The uncertainty assessment was based on 10% uncertainty of conversion coefficients (stated in ICRP report [15]), and

uncertainty of photon flux density described previously. These two main sources of final effective dose rate error have been treated as independent from each other.

2.2 α/β and γ laboratory spectrometry techniques

Nine rock samples collected in several points in Lab 2 and its surroundings (see: Fig. 2f) were prepared for laboratory gamma and alpha spectrometry analysis. Three samples were taken from rocks 50 m before the entrance to Lab 2 (from both sides of the corridor): PH-104 and PH-500907 (right side), PH-2229 (left side). Additional sample (PH-250907) was taken from the right side wall about 25 m from the door to Lab 2. This was done to investigate the homogeneity of radionuclide distribution in the rocks in the closest nearby of Lab 2. Samples collected in Hall 2 of Lab 2 contain concrete from wall coverage and wall material itself (PH-102 and PH-103). All rock samples were obtained by drilling from the first 10 m of the rocks. Collected samples were dried, crushed and homogenized. The gamma spectrometry measurements were carried out in polyethylene containers where samples were sealed for a month in order to obtain secular equilibrium in the uranium and thorium series. The measurements were performed with HPGe detectors having relative efficiencies from 25% to 37%. The acquisition and analysis of the spectra were performed with the use of Genie 2000^{TM} software. The energy calibration and activity concentrations of analyzed isotopes were obtained based on IAEA-RGTh-1, IAEA-RGK-1, IAEA RGU-1 reference materials. The activity concentration of ^{226}Ra isotope was calculated as the weighted mean of the activities of ^{214}Pb (295.2, 351.9 keV) and ^{214}Bi (609.3, 1120.3 keV), ^{232}Th (^{228}Ra) from ^{228}Ac (911.1 keV) and ^{212}Pb (238.6 keV), and ^{40}K from the 1460.8 keV line. For each sample, a separate sub-sample of a mass equal to about 2 g was prepared for α - spectrometric measurement. Rock samples were digested in PTFE pressure decomposition vessel. A microwave unit MAGNUM II (ERTEC-Poland) was used for heating the samples. Samples were spiked with ^{232}U isotope. The wet-mineralization of samples was performed with the use of hot acids: HF, HNO_3, HCl with H_3BO_3. Uranium was pre-concentrated with iron and co-precipitated with ammonia at pH 9. The separation of uranium from the other radionuclides was performed with the use of the anion exchange resin Dowex 1×8 (Cl^- type, 200-400 mesh) based on the procedure described in [16]. A thin α source was prepared from uranium fraction by coprecipitation with NdF_3 and filtration. The measurements of ^{234,238}U isotopes were performed with the use of α – spectrometer 7401VR (Canberra – Packard) equipped with a passivated implanted planar silicon detector with a surface area of 300 mm^2. Minimum detectable activity (MDA) was equal to 0.4 mBq per sample for both ^{234,238}U isotopes.

Three water samples were collected for the analysis of ^{226,228}Ra and ^{234,238}U isotopes. Two samples (PH-102 and PH-103) were taken from two separate pipes which collect the water seeping through the rocks behind Hall 2 of Lab 2, and the third sample (PH-500907) was collected directly from the rock outside Lab 2 in its nearby (~50 m before it). Samples straight after collection were acidified in order to avoid radionuclide precipitation as well as adsorption on the walls of the

containers. For uranium analysis, water samples were spiked with ^{232}U isotope of known activity. The separation of U was performed with the use of the anion exchange resin according to the same procedure as described for rock samples. For both ^{234,238}U isotopes, MDA was equal to 0.5 mBq/L and 0.5 L of the water initial sample volume. The chemical analysis of ^{226,228}Ra isotopes in investigated waters was based on the Polish Norm PN–89 Z–70072 (1989) [17]. The measurements with 1414 Win Spectral α/β LSC counter were performed once per day with 1 hour counting time for a period of one month. MDA was equal to 10 mBq/L and 30 mBq/L for ^{226}Ra and ^{228}Ra, respectively, for 1 h counting time and 2 L of water initial sample volume. The details about the applied spectrometry techniques are described elsewhere, e.g. [18,19].

2.3 Neutron flux measurements

The neutron detection setup used in the presented study was placed in the far right corner of Hall 2 in Lab 2 (Fig. 2). It consisted of ten bare ZDAJ NEM425A50 helium proportional counters (Fig. 2b), filled with ^{3}He at 4 atm, which are sensitive mainly to the thermal neutrons. Compared to the previous measurements [18] done in Freiberg within the BSUIN project, the number of helium counters was expanded. Counters were set in a flat vertical tray located parallel to the wall of the Hall 2, about 1 m away from it. Each counter is 50 cm long, has 2.5 cm in diameter, has its own independent electronics mounted in a brass tube, powered and controlled by the main PC via USB cable, i.e. is an independent, self-triggered measuring device. The operation method of this hardware was similar to that used previously in Freiberg [18], i.e. for each neutron event, the oscilloscope-like waveform was recorded, but the electronics were upgraded. The sampling rate was decreased to 1 MHz, but the length of the recorded wave-form could be remotely controlled and adjusted in a very wide range up to 10 000 samples. Remote control of the trigger level, the choice of one from a four predefined trigger position on the waveforms, and an analogue input amplifier gain have also been added. It was also possible to remotely upgrade the firmware of the device via an internet connection. The purpose of these improvements was the better adaptation of the measuring setup to the long-term remote-controlled operation. The features of the detection setup described above were useful during the calibration and adjustment of helium counters. During the measurements, the 50 samples waveforms (50 μs) were recorded, i.e. 20 samples before and 30 samples after the trigger (see: Fig. 3a). The data collection was 45.4 h due to relatively high counting rate. The analysis of the waveform shape (see: Fig. 3b) was used to reject non-neutron events occurring in helium counters. Such a signal has a rise time shorter than a neutron event.

The neutron signature in this kind of detectors is formed due to ^{3}He(n,p)^{3}H reaction, in which 764 keV of energy is released. The cross-section of this reaction is inversely proportional to the neutron energy, therefore only the thermal component of neutron flux could be measured efficiently with this method. The detailed characteristic of this detection setup is described elsewhere [18,20]. The characteristic structure of the helium counter spectrum is shown in Fig. 3c. On the ADC spectrum

also wall effect (connected with the escape of a part of the energy from the ^{3}He-n reaction) and alpha particle events from internal impurities of the counter body are also observed. The frequency of alpha particle interaction with ^{3}He in ZDAJ counters is about 3.2/h, and as a well-known effect could be used as an internal calibration source during low-rate neutron flux measurements. To determine the counting rate of neutron events, the pulse-shape analysis for each helium counter was applied. The cut-off threshold was based on the analysis of the maximal change in the signal during a rise time referred to the maximum amplitude of this signal (Fig. 3b). The effect of applying the cut-off threshold on the spectrum registered by helium counter is shown in Fig. 3c. Subsequently, for neutron events extracted from the spectrum of signal maximum amplitudes, a distribution of neutron counts over time was plotted separately for each helium counter. Then, the thermal neutron count rate was averaged over all detectors used, and the uncertainty of this result is a standard deviation of the mean value.

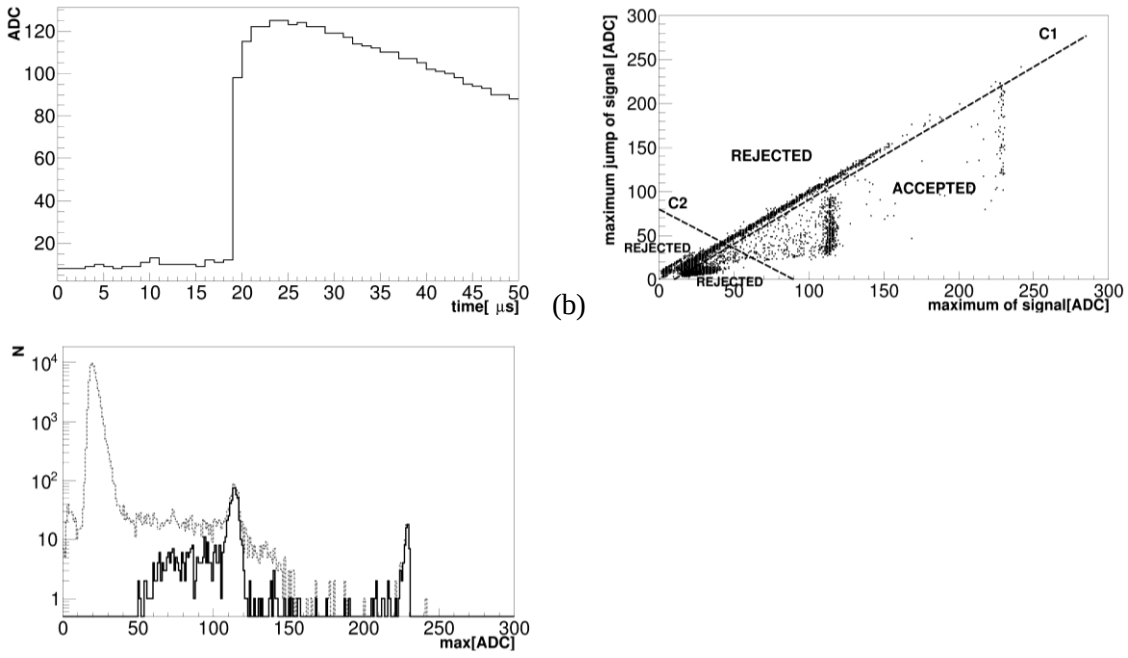

Figure 3. (a) An example of a single neutron event registration: oscilloscope like waveforms with 20 samples before and 30 samples after the trigger. (b) 2D histogram of the exclusion and inclusion regions of the pulse-shape analysis of neutron events. (c) The spectrum of signal maximum amplitudes registered in the helium counter: dashed line – without cut-off, solid line – with cut-off applied; around 115 ADC (764 keV) – deposition of a full energy of neutron interaction, 28 – 115 ADC (191 – 764 keV) – the "wall effect", 150 – 200 ADC alpha particle signal.

3. Results

In-situ gamma-ray spectrum presented in Fig. 4 was registered for 48 h during neutron flux measurements. The portable HPGe detector was placed in MP 1 (see: Fig. 2), a point located close to the detection setup for neutron flux investigations. Applying long counting time (from Saturday to Monday), allowed for the registration of both, the primary peaks with low statistical uncertainty, and low-intensity gamma rays, which are not often visible in underground locations. The summation lines in the high energy region (2650–3150 keV) and the characteristic X-rays for bismuth and lead are also

visible. These phenomena are a clear evidence of high ^{214}Bi concentration originating from ^{238}U isotope as a precursor of the uranium series.

The concentration of ^{222}Rn presented together with 2σ statistical uncertainty has been determined using RAD7 air-analyser. In MP1 it equals to 213.3 Bq/m^3 ± 11%, whereas 251.3 Bq/m^3 ± 11% was measured in MP2 and 270.4 Bq/m^3 ± 10% in MP3. The measurements lasted 24 – 48 h with 1-h sampling time and did not show any time-dependent structure. These findings are consistent with the previous in-air radon concentration measurements of 50 – 300 Bq/m^3 in the mine including the Hall 2 in Callio Lab 2 [14]. For comparison, the value of 233.3 Bq/m^3 ± 11% was measured in additional point outside the lab (near the point of a collection of a water sample). This suggests that concrete-coating of rock inside the Callio Lab 2 do not influence much the radon concentration. Comparing to the radon concentration in dwellings determined in indoor surveys given by UNSCEAR [21] as an arithmetic mean, which equals to 120 Bq/m^3 in Finland, at a depth of 1436 m in the Pyhäsalmi mine a two-fold increase in radon concentration is observed. The presence of ^{226}Ra line at the in-situ gamma-ray spectrum suggests that radon is not only transported with ventilation air but also originates from the uranium decay chain of radioisotopes incorporated in the rock. Typically radon concentration in the open air is 10 – 20 Bq/m^3, whereas in worldwide underground laboratories it was determined at the level of 33 – 120 Bq/m^3, except for Soudan UL, where seasonal variations between 300 and 700 Bq/m^3 were observed [2].

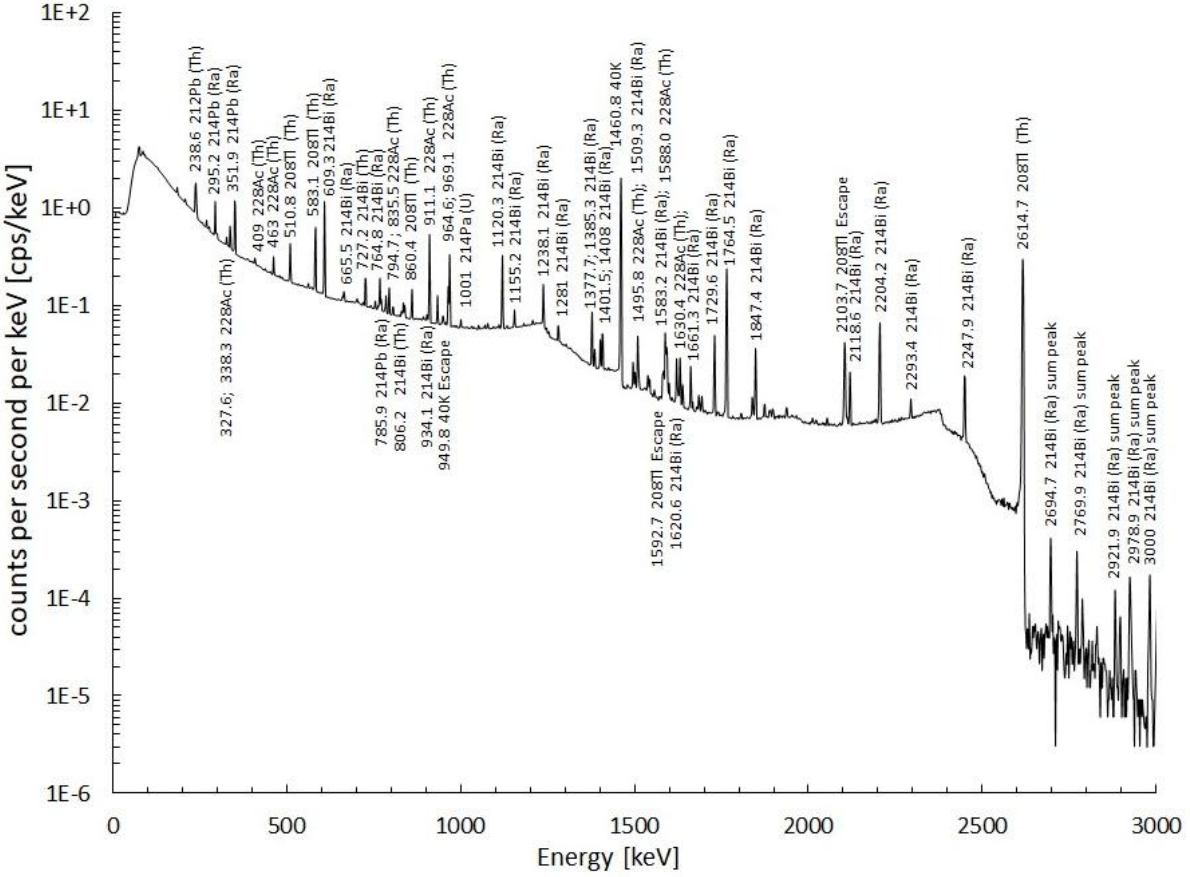

Figure 4. In-situ gamma-ray spectrum registered in the Hall 2 (MP 1) by the portable HPGe spectrometer within a 48-hour period. The main peaks are described. The presence of the escape peaks as well as the summation peaks indicates a relatively high level of radioactivity. The contribution to the effective dose of each radioisotope is presented in Table 2 together with detailed characteristics of count rates in particular spectral lines.

3.1 Quantitative analysis of the gamma-ray spectrum

The integral count rate on the spectrum up to 2700 keV equals to 654 ± 26 s^{-1} at the location of neutron flux investigation (MP1), whereas in MP2 and MP3 the values of 673 ± 26 s^{-1} and 517 ± 23 s^{-1}, respectively, were found. In other underground locations investigated previously it varies from 1.85 ± 0.02 s^{-1} in deep salt-rock location [22] through 107.86 ± 0.04 s^{-1} in deep calcschist-rock formation [23] to 371.50 ± 0.05 s^{-1} in shallow gneiss formation [18]. The photon flux density, assessed on the base of full-energy peaks, in MP 1 is 12.7 ± 1.5 $cm^{-2}s^{-1}$, and the total spectrum continuum (the total spectrum without full-energy peaks), which contains the contribution of the photons scattered inside the detector and the electromagnetic avalanche from the cosmic rays and their secondaries, is equal to 110.1 ± 12.4 $cm^{-2}s^{-1}$. For comparison purposes, the photon flux density in MP2 is 9.5 ± 1.3 $cm^{-2}s^{-1}$ and in MP3 is 5.5 ± 1.4 $cm^{-2}s^{-1}$, showing the walls as a primary gamma radiation source. These values are basically one order of magnitude higher than typical for the deep ULs, i.e. for locations deeper

than ~100 m photon flux depends on the local geology and typical values are of the order of 1 $cm^{-2}s^{-1}$ [3]. For instance, photon flux of 1.23 ± 0.17 $cm^{-2}s^{-1}$ is reported in LSC Canfranc [24], of 1.9 ± 0.4 $cm^{-2}s^{-1}$ in SURF Dakota [25], 2.16 ± 0.06 $cm^{-2}s^{-1}$ below 1300 m in Sanford Lab [26], 0.128 $cm^{-2}s^{-1}$ in Boulby [27], 0.301 – 0.622 $cm^{-2}s^{-1}$ in Modane [23], whereas in LNGS values of 0.25 – 1 $cm^{-2}s^{-1}$ are reported [28, 29].

The apparent activity of radionuclides, i.e. the radioactivity of isotopes incorporated in the wall materials (rocks and concrete coating), as seen by the spectrometer placed in the free air of the experimental hall (taking into account the gamma-ray absorption in the wall materials itself as well as the inverse square law factor) is at the level of 59 ± 17 Bq/cm^2 with the 51% contribution of ^{40}K, 21% of actinium series radionuclides, 18% of uranium-series radioisotopes and 10% of thorium decay chain nuclides. As concluded from previous studies at other underground localizations [18,30], the significant contribution to the measured signal from thorium series radionuclides is connected with the internal impurities of detection setup. The energies of radioisotopes recognized on the spectrum registered by 48-h in MP 1, count rate in each gamma line and radionuclides' contribution to the effective dose are presented in Table 2. The total effective dose was assessed at 0.158 ± 0.029 μSv/h in MP 1, 0.160 ± 0.032 μSv/h in MP 2 and 0.071 ± 0.007 μSv/h in MP 3. That means, the vicinity of the concrete-coated wall influences the estimation of radiation hazard.

Table 2. Counts per second of naturally occurring radionuclides as seen on the spectrum registered by the portable HPGe spectrometer and presented in Fig. 4, and their contribution to the effective dose in the point of measurement (MP 1).

Isotope (effective dose rate $\times 10^{-3}$ μSv/h)	Energy [keV]	Counts per second (cps)	Isotope (effective dose rate $\times 10^{-3}$ μSv/h)	Energy [keV]	Counts per second (cps)
Thorium decay chain			K-40 (55.05 ± 7.79)	1460.8	5.702 ± 0.006
Tl-208 (34.76 ± 0.40)	211.4	0.038 ± 0.008	Uranium decay chain		
	233.4	0.050 ± 0.004	Ra-226 (0.14 ± 0.01)	186.1	0.589 ± 0.011
	252.6	0.022 ± 0.004	Th-234 (0.07 ± 0.01)	63.3	0.084 ± 0.016
	277.3	0.161 ± 0.004		92.6	0.596 ± 0.008
	510.8	0.739 ± 0.005	Pa-234 (0.18 ± 0.03)	1001.0	0.035 ± 0.002
	583.2	1.582 ± 0.005	Pb-214 (3.73 ± 0.68)	242.0	0.893 ± 0.005
	763.1	0.026 ± 0.001		274.5	0.029 ± 0.003
	860.6	0.203 ± 0.003		295.2	1.501 ± 0.005
	1093.9	0.013 ± 0.003		351.9	2.712 ± 0.008
	2614.5	1.109 ± 0.003		487.1	0.032 ± 0.002
Pb-212 (1.37 ± 0.82)	115.2	0.062 ± 0.015		533.7	0.011 ± 0.004
	238.6	3.280 ± 0.006		785.9	0.113 ± 0.002
	300.1	0.224 ± 0.003	Bi-214 (41.4 ± 16.6)	387.0	0.022 ± 0.002
Bi-212 (1.90 ± 0.15)	288.1	0.012 ± 0.006		389.1	0.032 ± 0.003
	452.8	0.022 ± 0.004		609.3	2.639 ± 0.006
	727.2	0.342 ± 0.002		665.4	0.091 ± 0.002

	893.4	0.016 ± 0.003		697.9	0.004 ± 0.002
	1078.6	0.021 ± 0.001		703.1	0.034 ± 0.002
	1620.5	0.055 ± 0.001		719.9	0.023 ± 0.001
	1806.0	0.0035 ± 0.0002		768.4	0.274 ± 0.002
Ac-228	99.5	0.127 ± 0.013		806.2	0.068 ± 0.003
(17.72 ± 2.51)	129.1	0.218 ± 0.012		934.1	0.160 ± 0.003
	154.0	0.117 ± 0.010		1052.0	0.018 ± 0.002
	209.2	0.299 ± 0.010		1070.0	0.011 ± 0.001
	270.2	0.300 ± 0.004		1120.3	0.735 ± 0.004
	321.6	0.016 ± 0.005		1133.7	0.008 ± 0.002
	327.6	0.195 ± 0.003		1155.2	0.088 ± 0.003
	332.4	0.016 ± 0.003		1207.7	0.021 ± 0.003
	338.3	0.731 ± 0.004		1238.1	0.297 ± 0.002
	409.5	0.119 ± 0.003		1281.0	0.065 ± 0.002
	463.0	0.276 ± 0.005		1377.7	0.187 ± 0.001
	478.3	0.030 ± 0.002		1385.3	0.040 ± 0.001
	562.5	0.043 ± 0.004		1401.5	0.063 ± 0.001
	674.6	0.007 ± 0.003		1408.0	0.112 ± 0.001
	707.4	0.012 ± 0.002		1509.2	0.095 ± 0.001
	755.3	0.050 ± 0.002		1538.5	0.019 ± 0.001
	772.3	0.073 ± 0.002		1543.3	0.013 ± 0.001
	782.1	0.021 ± 0.001		1583.2	0.0339 ± 0.0004
	794.9	0.211 ± 0.004		1599.3	0.0146 ± 0.0003
	830.5	0.031 ± 0.001		1661.3	0.046 ± 0.001
	835.7	0.083 ± 0.002		1684.0	0.011 ± 0.001
	840.4	0.073 ± 0.002		1729.6	0.127 ± 0.001
	904.2	0.036 ± 0.001		1764.5	0.683 ± 0.002
	911.2	1.218 ± 0.003		1838.4	0.014 ± 0.001
	958.6	0.009 ± 0.001		1847.4	0.088 ± 0.001
	964.8	0.244 ± 0.002		1873.2	0.009 ± .0.001
	969.0	0.727 ± 0.002		1896.3	0.009 ± 0.001
	988.4	0.011 ± 0.002		2052.9	0.003 ± 0.001
	1110.6	0.014 ± 0.002		2110.0	0.0044 ± 0.0005
	1247.1	0.016 ± 0.001		2118.5	0.050 ± 0.001
	1495.9	0.034 ± 0.001		2204.2	0.207 ± 0.002
	1501.6	0.016 ± 0.001		2293.4	0.013 ± 0.001
	1557.1	0.007 ± 0.001		2447.9	0.062 ± 0.001
	1580.5	0.0220 ± 0.004	Characteristic X-rays (0.70 ± 0.10)		
	1588.2	0.131 ± 0.001	Pb – $K_{\alpha 1}$	75.0	1.870 ± 0.009
	1625.0	0.011 ± 0.001	Pb – $K_{\beta 1}$	84.9	0.658 ± 0.008
	1630.6	0.063 ± 0.001	Bi – $K_{\alpha 1}$	77.1	2.514 ± 0.010
	1638.3	0.020 ± 0.001	Bi – $K_{\beta 1}$	87.3	1.244 ± 0.008
	1666.5	0.0055 ± 0.0005	Tl – $K_{\beta 1}$	82.6	0.266 ± 0.008

	1887.1	0.007 ± 0.001	Ac – $K_{\alpha 1}$	90.9	0.740 ± 0.008
Actinium decay chain			Th – $K_{\beta 1}$	105.6	0.104 ± 0.014
Pb-211 (0.014 ± 0.004)	404.9	0.013 ± 0.002			
U-237 (0.050 ± 0.009)	33.2	0.079 ± 0.008			
	164.6	0.032 ± 0.012			
	267.5	0.073 ± 0.005			
Ra-223 (0.009 ± 0.001)	144.2	0.057 ± 0.013			
U-239 (0.094 ± 0.004)	662.2	0.037 ± 0.002			

3.2 Ratio of K-40/Bi-214

As in the previous paper describing radiation environment at TU Bergakademie in Freiberg [18] the ratio of count rates under the peaks of 1460.8 keV and 1764.5 keV from ^{40}K and ^{214}Bi, respectively, was assessed. The values of 8.35 ± 0.01, 8.18 ± 0.01 and 11.91 ± 0.04 for Callio Lab 2 MP 1, MP 2 and MP 3, respectively, are higher than the values reported for other deep ULs and are closer to those from a shallow localization of e.g. Reiche Zeche shaft at TUBAF in Germany [18]. For example, at the Sanford Underground Research Facility (SURF) located in a volcanic rock with rhyolite intrusions in halls covered by a layer of sprayed shotcrete ^{40}K/^{214}Bi ratio is 8.86 – 9.66 [25]; at Gran Sasso LNGS laboratory in dolomitic limestone covered by concrete it is 2 – 6.2 depending on the season [31]; at LSC in Canfranc laboratory in calize rock, which is a calcium carbonate with traces of quartz, it is 5 [32]; in salt rock surrounded by anhydrite layer it is around 3.3 [22]. From this short overview, it seems that the combination of volcanic rock and shotcrete wall coverage is responsible for ^{40}K/ ^{214}Bi > 8 for depths greater than 1 km w.e.

3.3 Radioactivity content in rocks and water

The data from the atlas of the *Forum of European Geological Surveys* (FOREGS) [33] concerning uranium, thorium and potassium concentrations in the subsoil of Pyhäsalmi mine region (63.95 latitude and 26.25 longitude) are the following: 1.12 ppm of U, 4.36 ppm of Th and 1.81% of K. Hence, the radioactivity concentrations are the following: 13.8 Bq/kg for ^{238}U, 17.7 Bq/kg for ^{232}Th and 286 Bq/kg for ^{40}K. The activity concentrations of ^{226}Ra, ^{232}Th, ^{40}K obtained from laboratory gamma spectrometric measurements are presented in Table 3. The concentrations of analyzed isotopes varied greatly depending on the place of sample collection in Lab 2, and the mean values (average ± SD) of 45.6 ± 68.5 Bq/kg, 25.3 ± 20.8 Bq/kg and 453.8 ± 339.6 Bq/kg were obtained for ^{226}Ra, ^{232}Th and ^{40}K, respectively. Since the deviation from sample to sample are large, the average values stated for the whole mine of 0.8 ppm U and 3.2 ppm Th [14] should not be applied for the prediction of radiation conditions in studied localization of Callio Lab 2. The results of alpha spectrometry measurements in rock samples are presented in Table 4. The concentrations varied in the range from 1.4 ± 0.2 Bq/kg to 211 ± 10 Bq/kg and from 1.6 ± 0.2 Bq/kg to 212 ± 10 Bq/kg for ^{234,238}U, respectively. The highest uranium content, calculated based on the uranium concentration, was equal

to 17.08 ± 0.77 ppm. In analyzed samples, ^{234}U and ^{238}U isotopes are in radioactive secular equilibrium and $^{234}U/^{238}U$ activity ratios, within the estimation of uncertainty, were equal to 1. On the other hand, $^{226}Ra/^{238}U$ activity ratio varied in a range from 0.70 ± 0.05 to 13.66 ± 2.03, which means, a part of the rock samples showed disequilibrium between ^{238}U and ^{226}Ra isotopes. Sometimes building materials (i.e. cement, bricks) contain industrial wastes and ashes from conventional furnaces. It is known, that during coal combustion disequilibrium between isotopes from uranium and thorium series may occur and the same isotopes are portioned between fly and bottom ashes. These findings confirm quite large differences in the content of concrete used to cover floor and walls, since the natural radioactivity in floor material was of higher concern during Hall 2 preparation and therefore is at a lower level, whereas walls were prepared prior to the establishment of the Lab 2 and therefore covered by the shotcrete with a relatively high content of natural radioactivity at the levels of 140 ± 11 Bq/kg ^{40}K, 160 ± 32 Bq/kg ^{226}Ra and 240 ± 19 Bq/kg ^{232}Th [14].

Table 3. Radioisotopes activity concentrations as a result of the analysis of rock samples with the use of gamma spectrometry technique in laboratory conditions.

Sample	Activity concentration [Bq/kg]		
	^{226}Ra	^{232}Th (^{228}Ra)	^{40}K
PH-102	19.1 ± 0.8	6.8 ± 0.5	104 ± 10
Concrete samples of the floor material used in Lab 2	34.9 ± 1.0	23.6 ± 1.1	484 ± 37
Wall shotcrete, left side of Lab 2	40.2 ± 1.6	53.8 ± 3.1	662 ± 53
Wall shotcrete, right side of Lab 2	91.0 ± 2.4	34.4 ± 1.5	1136 ± 47
R-2229	32.7 ± 0.9	8.2 ± 0.4	256 ± 20
PH-500907	58.0 ± 2.3	46.6 ± 2.4	272 ± 24
PH-250907	10.6 ± 0.6	3.7 ± 0.4	122 ± 12
PH-104	8.1 ± 0.4	2.6 ± 0.3	302 ± 24
PH-103	188.2 ± 5.1	47.8 ± 2.0	746 ± 56

Table 4. Radionuclide content in rock samples obtained with the use of alpha spectrometry technique. The results are presented in terms of uranium activity concentration, uranium content, and $^{234/238}U$, $^{226}Ra/^{238}U$ activity ratios.

Sample	Radionuclide content				
	^{238}U [Bq/kg]	^{234}U [Bq/kg]	U [ppm]	$^{234}U/^{238}U$	$^{226}Ra/^{238}U$
PH-102	1.4 ± 0.2	1.6 ± 0.2	0.11 ± 02	1.14 ± 0.19	13.66 ± 2.03
Concrete samples of the floor material used in Lab2	25.8 ± 1.6	24.1 ± 1.5	2.17 ± 0.16	0.94 ± 0.10	1.35 ± 0.09
Wall shotcrete, left side of Lab2	57.4 ± 3.7	53.9 ± 3.5	4.46 ± 0.30	0.94 ± 0.09	0.70 ± 0.05
Wall shotcrete, right side of Lab2	87.1 ± 3.6	89.2 ± 3.7	7.05 ± 0.30	1.02 ± 0.60	1.04 ± 0.05
R-2229	11.4 ± 1.4	10.3 ± 1.3	0.93 ± 0.11	0.90 ± 0.15	2.86 ± 0.36
PH-500907	4.3 ± 0.5	5.2 ± 0.5	0.53 ± 0.04	1.20 ± 0.17	13.49 ± 1.66

PH-250907	6.4 ± 0.8	6.9 ± 0.8	0.50 ± 0.04	1.07 ± 0.18	1.66 ± 0.23
PH-104	5.8 ± 0.4	6.0 ± 0.4	0.47 ± 0.03	1.03 ± 0.09	1.39 ± 0.12
PH-103	211 ± 10	212 ± 10	17.08 ± 0.77	1.00 ± 0.06	0.89 ± 0.05

The results of the analysis of uranium and radium in water samples are presented in Table 5. Two samples, obtained in Hall 2 Lab 2, showed uranium ^{238}U concentrations below 0.5 mBq/L. For water sample collected outside Callio Lab 2 (PH-500907) uranium content is equal to 0.53 ± 0.05 µg/L. This water also showed disequilibrium between ^{234,238}U isotopes. Disequilibrium between these two isotopes in underground water is a common phenomenon and processes responsible for that are reviewed e.g. in [34]. On the other hand, all water samples showed ^{226}Ra, ^{228}Ra concentrations above the limit of detections. This may indicate that there are favorable conditions for water to receive the radium isotopes from reservoir rocks or rocks are rich in radioactive content.

Table 5. Activity concentrations of uranium and radium isotopes analyzed in water samples with the use of LSC counter and alpha-spectrometry techniques.

Sample	^{238}U [mBq/L]	^{234}U [mBq/L]	U [µg/L]	^{238}U/^{234}U	^{226}Ra [Bq/L]	^{228}Ra [Bq/L]
PH-500907	6.5 ± 0.7	11.1 ± 0.9	0.53 ± 0.05	1.70 ± 0.23	54.9 ± 1.3	36.0 ± 2.8
PH-102	<0.5	4.9 ± 0.7			116.6 ± 2.7	10.7 ± 4.5
PH-103	<0.5	0.8 ± 0.2			15.1 ± 0.4	6.1 ± 0.9

3.4 Qualitative neutron activation analysis

All of 146 spectral lines observed at the spectrum measured in-situ in Callio Lab 2 (MP1) and shown in Fig. 4, were identified as natural background radiation from natural radioactive chains (decay gammas and characteristic X-rays) and potassium K-40. Nevertheless, the investigation of the potential neutron-induced radionuclides was made. Such radioisotopes could be activated if the neutron flux would be more intense and therefore could affect gamma-energy spectrum and contribute to the radiation hazard in this localization. A rock sample from the wall of experimental Hall in Lab 2 (Hall 2 in Fig. 2) was irradiated by neutron flux of about 10^5 n/cm^{2}s from a ^{252}Cf source for approximately one month. This means, the neutron flux was 10 orders of magnitude higher than that measured in MP1. Subsequently, the gamma-ray spectrum of an activated sample was registered using a HPGe detector, the same laboratory setup as for radioisotopes concentration analysis. As a result of the neutron capture process (n,γ), secondary decay gamma radiation from ^{24}Na, ^{28}Al, ^{56}Mn, ^{46}Sc, ^{59}Fe and ^{60}Co was observed. This suggests that potentially neutron-induced gamma radiation originates in the activated admixtures in the rock of Pyhäsalmi region as well as in one of the main elements (iron in ferrite). Photon energies are within the range from 847 keV (^{56}Mn) to 2754 keV (^{24}Na). Among the activated radionuclides, only scandium is not the main component or metal admixture in rock types of Pyhäsalmi region, listed in Table 1. However, this element can be found in chalcopyrite, but does not

belong to the common additives. Measurable effect of neutron activation in laboratory conditions shows a relatively high concentration of scandium in studied rock samples.

The count rates in activation saturation conditions were in the range of $10^{-3} – 10^{-1}$ s^{-1}. Since the neutron flux during in-situ measurements in MP1 was about 10 orders of magnitude lower than that used in laboratory conditions, one may expect the count rates at a level of $10^{-13} – 10^{-10}$ s^{-1} in Hall 2 of Lab 2 assuming the activation, which contribute to the registered gamma-ray spectrum, occurs at the first few centimetres of rock, i.e. self-attenuation is negligible. For non-low-background equipment this is far below the detection limit. However, in low-background experiments it could be not-negligible.

3.5 Neutron flux results

The calculation of neutron flux was based on the neutron counting rate in each of helium counters (Tab. 6) and the Monte Carlo simulations of detector response in a known isotropic thermal neutron flux. GEANT4 version 10.04 with QGSP_BERT_HP and Neutron HP Thermal Scattering packages was used. The coefficient as a ratio of simulated response of the detector (counting rate) and simulated neutron flux was then applied as the detection efficiency coming from the computer simulations, to convert the value of measured neutron counting rate (Fig. 5a) to neutron flux density [$s^{-1}cm^{-2}$] (Fig. 5b). The distribution of neutron events over measuring time, as exemplary presented in Fig. 5a, showed good stability of the signal for each of helium counter.

(a) 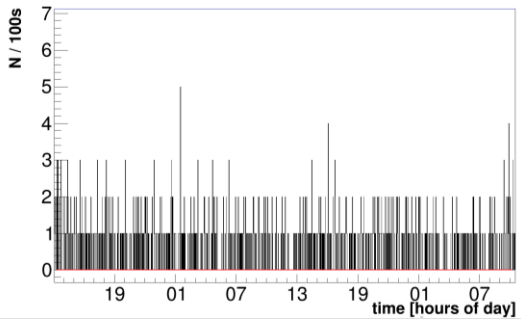

(b) 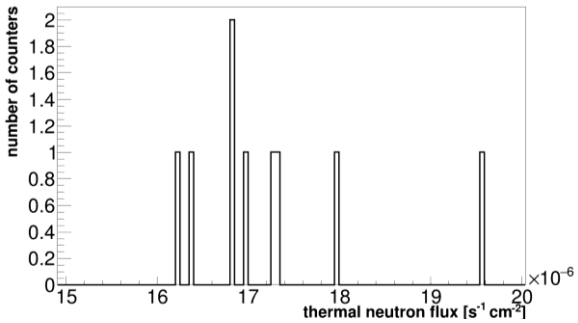

Figure 5. (a) Exemplary distribution of neutron events over measuring time as seen by a single helium counter and (b) distribution of thermal neutron flux for the entire detection setup.

The final thermal component of neutron flux was $(1.73 \pm 0.10) \times 10^{-5}$ $cm^{-2}s^{-1}$, obtained as the average from the results for each helium counter, as presented in Table 6. This value is higher than for any other location studied using the ZDAJ detection setup, as presented in Table 7.

Table 6. Neutron count rate as seen by each of helium counters and the corresponding neutron flux. The uncertainties are the result of the precision of fitting linear functions to the distributions of counts over time. Detector number is determined by the counter position in a tray (see: Fig. 2b). The result from detector #3 was not taken into account as the counter became damaged during measurements.

Detector number	Neutron count rate per 1 hour	Neutron flux $\times 10^{-5}$ [$cm^{-2}s^{-1}$]
1	13.9 ± 0.5	1.62 ± 0.06
2	14.8 ± 0.5	1.73 ± 0.06
3	breakdown	—
4	14.4 ± 0.5	1.68 ± 0.06
5	14.8 ± 0.5	1.73 ± 0.06
6	14.5 ± 0.5	1.70 ± 0.06
7	15.4 ± 0.6	1.80 ± 0.06
8	14.4 ± 0.5	1.68 ± 0.06
9	14.0 ± 0.5	1.64 ± 0.06
10	16.8 ± 0.6	1.96 ± 0.08

The previous investigations of the neutron flux at the level of 1410 m in Pyhäsalmi mine [35] gives the results of $(42.2 \pm 5.0) \times 10^{-7}$ $cm^{-2}s^{-1}$, $(16.8 \pm 5.8) \times 10^{-7}$ $cm^{-2}s^{-1}$ and $<1.6 \times 10^{-7}$ $cm^{-2}s^{-1}$ for energy regions of <1.5 MeV (including thermal neutrons also measured in presented study), 1.5 – 12 MeV (fast neutrons produced in (α,n) reactions) and >12 MeV (muon-induced neutrons). In deep underground locations, the primary mechanism of neutron production is (α,n) reaction, followed by fission process, and muon-induced neutrons are of minor importance due to decreasing of muon intensity at large in-rock depths. Therefore, the originated neutron spectrum is peaked around 1 – 2 MeV. However, in-cavern measurement influences on neutron spectrum to a large extent since a significant thermal component of neutron flux occurs. Some investigations demonstrate that the component below ~1.5 MeV might have up to about 70% contribution in a total neutron flux in deep underground locations [35,36]. The results presented here, in comparison with that, reported earlier for Pyhäsalmi mine [35] (localization different than Lab 2) confirms these findings since the thermal neutron flux component measured in the vicinity of the concrete-coated wall is about 75% higher than neutron flux with E < 1.5 MeV obtained at similar depth in this mine [35] but for different measuring point surroundings. Large differences in obtainable results are also pointed out by other investigators [26,36,37] paying attention mostly to the uranium and thorium concentration in materials surrounding the experimental hall. Also, the vicinity of walls coated with concrete (hall dimensions) are mentioned as a factor increasing the low-energy component of neutron flux [38].

Table 7. Comparison of thermal neutron flux measurement performed using ZDAJ helium counters setup in different European underground locations.

Location	Depth	Surrounding rocks	Thermal neutron flux $\times 10^{-6}$ [$cm^{-2}s^{-1}$]
Gran Sasso, Italy [39]	1400 m (3800 m w.e.)	limestone	0.56 ± 0.23
Slanic Prahova, Romania [39]	208 m (600 m w.e.)	salt	0.12 ± 0.05
Freiberg, Germany [18]	150 m (410 m w.e.)	gneiss	3.12 ± 0.10
Pyhäsalmi, Finland	1436 m (4000 m w.e.)	granite	17.30 ± 1.00

4. Discussion and Conclusions

Gamma-ray flux of 12.7 ± 1.5 $cm^{-2}s^{-1}$ and neutron flux of $(1.73 \pm 0.10) \times 10^{-5}$ $cm^{-2}s^{-1}$, measured in Callio Lab 2, are directly dependent on the U and Th concentrations in rocks, which were determined in the range of 0.11 – 17.08 ppm and 0.64 – 13.23 ppm, respectively. The natural radiation

background characterized by the gamma-radiation dose rate, here at the level of 0.158 ± 0.029 μSv/h, and radon concentration, here of 213.3 ± 23.5 Bq/m^3, in halls prepared for experimental use is modified by the presence of additional coating materials, e.g. shotcrete, could be not negligible even in deep located laboratories. The main contributors to the effective dose are ^{40}K (35%), ^{214}Bi (26%), from uranium series and ^{208}Tl (22%) from thorium series. This is also due to the relatively high concentration of potassium ^{40}K of 104 – 1136 Bq/kg, as measured in rock samples.

The uranium and thorium concentration and thus, neutron production yield deep underground is relatively high for granite rock types, where 1.32 – 6.25 ppm U, 4.38 – 11 ppm Th and 7.3 – 17.9 neutrons/g/y is reported e.g. in [37]. In limestone and sandstone rock types the concentrations of U and Th are about 1 ppm and neutron yield about 1.5 n/g/y [37]. The concentration of uranium in salt rock type is usually below 1 ppm, but since the concentration of thorium is about 2 ppm, the neutron yield could reach 3.6 – 6.5 n/g/y [37, 40]. Higher values of 44.13 ppm U and 6.83 ppm Th in gneiss could result in 61.2 n/g/y of neutron production [40]. As reported in [27], halite rock contains 32 ± 7 ppb of ^{238}U and 160 ± 20 ppb of ^{232}Th, which could result in neutron yield of the order of 1 n/g/y provided that the data given in [37] are linearly dependent. Lab 2 is surrounded by felsic volcanic bedrock with a volcanogenic massive sulphide deposit and additionally covered by various types of concrete from the inside (with increased concentration of natural radionuclides, as our analysis has shown). Therefore, based on the average uranium and thorium concentrations in rocks measured in the presented study (3.69 ppm U and 6.22 ppm Th), the neutron yield produced via (α,n) and uranium fission mechanisms might be of the order of 12.2 n/g/y if the relationship given in [37] is linear.

The muon flux measurements in Pyhäsalmi mine [8] show a clear dependence on the w. e. depth. The value of (1.1 ± 0.1) × 10^{-8} cm^{-2}s^{-1} obtained closest to the location of environmental radioactivity investigations in Callio Lab 2 is about 40% higher than the result of calculation based on the semi-empirical formulae [7,37,41] from the literature, which give the results within the range of (6.1 ÷ 6.8) × 10^{-9} cm^{-2}s^{-1}sr^{-1}. The similar value of 6.27 × 10^{-9} cm^{-2}s^{-1}sr^{-1} is also given by Kudryavtsev et al. for the depth of 4 km w.e [42]. However, every empirical formula, as well as Monte Carlo simulations are very sensitive on the rock composition [43]. Therefore the results of measurements for the Pyhäsalmi mine at the 1436 m depth level could be different from the calculated predictions made for the "ordinary rocks" [43] taking into account specific local geology (see: subsection 1.1). Moreover, since the Pyhäsalmi mine is still operational, significant changes in densities occur, i.e. a lot of extracted ore was replaced with less dense material to stabilize the geology. Therefore, the predictions of muon flux based on the depth and rock densities at a present-day are probably underestimated.

Muon induced neutron flux at a given w.e. depth was estimated using a fitting function for literature data, as analysed in [7]. According to the relation given therein, the muon-induced neutron flux in studied localization of Callio Lab 2 in Pyhäsalmi mine at 4000 m w.e. is of the order of (8.21 ± 3.15) × 10^{-10} cm^{-2}s^{-1}, where the uncertainty was calculated based on the uncertainties of fitting parameters

presented in [7]. Neutron flux originated from the (α,n) reactions is independent on the depth and thus, as mentioned above, is related to the U/Th concentrations in rocks, whereas muon-induced neutron flux is strongly depth-dependent. Therefore, the difference of three orders of magnitude is expected [7,42] for deep ULs (~3 km w.e. coverage) between the total measured neutron flux and muon-induced neutrons. Almost five orders of magnitude difference obtained in the presented study indicates that Lab 2 of Callio Lab in Pyhäsalmi mine could be perceived as deep location, since high concentration of uranium and thorium in concrete-coating of Hall 2 walls results in the thermal neutron flux at the high level of $(1.73 \pm 0.10) \times 10^{-5}$ $cm^{-2}s^{-1}$. The same order of magnitude is reported for neutron flux in Yangyang (Korea), Jinping (China), Kamioka (Japan), and Canfranc (Spain) underground laboratories [44,45], which are located at shallower depths of 2000 – 2700 m w.e. At the depth larger than 4000 m w.e. about two-times lower values are reported, e.g. for SNOLAB in Canada [24] and SURF laboratory where low energy neutron flux was measured [38].

The issue of doses in underground experimental halls is usually of minor concern and is rarely studied, even when muon, neutron and gamma-ray fluxes are deeply investigated [1,2]. Nevertheless, it is important both, from the point of view of radiation hazard (when there is a supposition about an increased level of radioactivity e.g. in concrete materials), and when characterising the background for biological experiments. The absorbed dose in the air in Finland as shown in UNSCEAR report [21] ranges from 0.022 to 0.184 μGy/h taking into account outdoors and indoors expositions, which gives the range of 0.026 – 0.222 μSv/h of the radiation hazard. From the underground laboratories, there are scarce literature information about dose estimations. Among them, LSM in Modane localized in calcschist rock concrete-coating shows the gamma background dose at the level of 20 nSv/h [5], Jinping in marble rock shows 23.22 nSv/h [46], Slanic Prahova, Romania in salt rock reported up to 2.56 ± 0.55 nSv/h [47], salt cavern in Sieroszowice, Poland – 2.1 nSv/h [22], and Asse salt mine, Germany 1.3 nSv/h [48]. The result of 0.158 ± 0.029 μSv/h obtained on the base of the gamma-ray spectrum registered in MP 1 in Callio Lab is within the range reported by UNSCEAR for the ground locations in Finland.

Acknowledgements

This study was performed under the Baltic Sea Underground Innovation Network (BSUIN) project, which is supported by the EU's Interreg Baltic Sea Region Programme.

References

[1] L. Pandola, Overview of the European Underground Facilities. AIP, Conf. Proc. 1338 (2011) 12.

[2] A. Bettini, The world underground scientific facilities. A compendium. arXiv:0712.1051, (2007).

[3] A. Bettini, The world deep underground laboratories. Eur. Phys. J. Plus, 127(9) (2012) 114.

[4] A. Ianni, Review of technical features in underground laboratories. International Journal of Modern Physics, 32(30) (2017) 1743001.

[5] N. Lampe, P. Marin, J. Castor, G. Warot, S. Incerti, L. Maigne, D. Sarramia, V. Breton, Background study of absorbed dose in biological experiments at the Modane Underground Laboratory. EPJ Web of Conferences 124 (2016) 00006.

[6] E. Coccia, Underground Laboratories: cosmic silence, loud science, Journal of Physics: Conference Series 203 (2010) 012023.

[7] D.M. Mei, A. Hime, Muon-induced background study for underground laboratories, Phys Rev D 73 (2006) 053004.

[8] T. Enqvist, A. Mattila, V. Foehr, T. Jamsen, M. Lehtola, J. Narkilahti, J. Joutsenvaara, S. Nurmenniemi, J. Peltoniemi, H. Remes, J. Sarkamo, C. Shen, I. Usoskin, Measurements of muon flux in the Pyhasalmi underground laboratory. Nucl. Instrum. Methods Phys. Res. A 554(1-3) (2005) 286-290.

[9] T. Mäki, J.Kousa, J. Luukas, The Vihanti-Pyhäsalmi VMS Belt, in: W. Maier, R. Lahtinen, H. O'Brien (Eds.), Mineral deposits of Finland. Elsevier, Amsterdam (2015) 507-530.

[10] I. Kukkonen, P. Heikkinen, S. Heinonen, J. Laitinen and HIRE Working Group of the Geological Survey of Finland, HIRE Seismic Reflection Survey in the Pyhäsalmi Zn-Cu mining area, central Finland, Geological Survey of Finland, Geophysical research report Q 23/2009/43 (2009) 49. http://tupa.gtk.fi/raportti/arkisto/q23_2009_43.pdf

[11] H. Puustjärvi (ed.), Pyhäsalmi modeling project 13.5.1997 - 12.5.1999, Outokumpu Mining Oy & Geological Survey of Finland, M19/3321/99/1/10 (2006).
http://tupa.gtk.fi/raportti/arkisto/m19_3321_99_1_10.pdf

[12] R.B. Firestone, V.S. Shirley, Tables of Isotopes, John Wiley & Sons Inc, New Jersey, 1996.

[13] Kalliosuunnittelu Oy Rockplan Ltd , Deliverable 7 Geological modelling, LAGUNA-LBNO Extended site investigation at Pyhäsalmi, Finland (2014).

[14] J. Joutsenvaara, Deeper understanding at Lab 2: the new experimental hall at Callio Lab underground centre for science and R & D in the Pyhäsalmi Mine, Finland. Master's thesis, Oulu University, 2016.

[15] N. Petoussi-Henss, W.E. Bolch, K.F. Eckerman, A. Endo, N. Hertel, J. Hunt, M. Pelliccioni, H. Schlattl, M. Zank, ICRP publication 116: Conversion coefficients for radiological protection quantities for external radiation exposures, Ann. ICRP 40 (2–5) (2010) 1–257,
http://dx.doi.org/10.1016/j.icrp.2011.10.001.

[16] J. Suomela, Method for determination of U-isotopes in water, Swedish Radiation Institute, Stockholm, SSI-rapport, 0282-4434, 93:14 (1993).

[17] Polish Norm PN-89/ZN-70072, Radium isotopes determination in water with LSC method, Wydawnictwa Normalizacyjne Alfa, Warszawa, 1989 (in Polish).

[18] K. Polaczek-Grelik et al, Characterization of the radiation environment at TU Bergakademie in Freiberg, Saxony, Germany. Nuclear Instruments and Methods in Physics Research A, 946 (2019) 162652 .

[19] A. Walencik-Łata, B. Kozłowska, J. Dorda, T.A. Przylibski, The detailed analysis of natural radionuclides dissolved in spa waters of the Kłodzko Valley, Sudety Mountains, Poland. Science of the total Environment, 569-570 (2016) 1174-1189.

[20] Z. Dębicki, K. Jędrzejczak, M. Kasztelan, W. Marszał, J. Orzechowski, J. Szabelski, P. Tokarski, The BSUIN Project – overview and same results. IOP Conf. Series: Journal of Physics: Conf. Series 1181 (2019) 012071.

[21] United Nations Scientific Committee on the Effects of Atomic Radiation: Sources and Effects of Ionizing Radiation. UNSCEAR 2000 Report to the General Assembly, with Scientific Annexes. New York, 2000.

[22] J. Kisiel, M. Budzanowski, J. Dorda, K. Kozak, J. Mazur, J.W. Mietelski, M. Puchalska, E. Tomankiewicz, A. Zalewska, Measurements of natural radioactivity in the salt cavern of the Polkowice-Sieroszowice copper mine. Acta Phys Pol B 41(7) (2010) 1813-1819.

[23] D. Malczewski, J. Kisiel, J. Dorda, Gamma background measurements in the Laboratoire Souterrain de Modane. J Radioanal Nucl Chem 292 (2012) 751–756.

[24] A. Bettini, New underground laboratories: Europe, Asia and the Americas. Physics of the Dark Universe 4 (2014) 36–40.

[25] D.S. Akerib, C.W. Akerlof, S.K. Alsum, N. Angelides, H.M. Araujo, J.E. Armstrong, M. Arthurs, X. Bai, J. Balajthy, S. Balashov, A. Baxter, E.P. Bernard, A. Biekert, T.P. Biesadzinski, K.E. Boast, B. Boxer, P. Bras, J.H. Buckley ... J. Yin, Measurement of the gamma ray background in the Davis Cavern at the Sanford Underground Research Facility. Astroparticle Physics 116 (2020) 102391, https://doi.org/10.1016/j.astropartphys.2019.102391.

[26] D.-M. Mei, C. Zhang, K. Thomas, F. Gray, Early Results on Radioactive background characterization for Sanford Laboratory and DUSEL Experiments. Astroparticle Physics 34(1) (2010) 33-39.

[27] D. Malczewski, J. Kisiel, J. Dorda, Gamma background measurements in the Boulby Underground Laboratory. J Radioanal Nucl Chem 298 (2013) 1483–1489.

[28] D. Malczewski, J. Kisiel, J. Dorda, Gamma background measurements in the Gran Sasso National Laboratory. J Radioanal Nucl Chem 295 (2013) 749–754.

[29] M. Haffke, L. Baudis, T. Bruch, A.D. Ferella, Marrodan Undagoitia T, Schumann M, Te Y.-F, van der Schaaf A, Background measurements in the Gran Sasso Underground Laboratory. Nucl. Instrum. Methods Phys. Res. A 643(1) (2011) 36–41.

[30] K. Polaczek-Grelik, J. Kisiel, A. Walencik-Łata, J.W. Mietelski, P. Janowski, M. Harańczyk, J. Jurkowski, A. Zalewska, J. Kobziński, P. Markowski, A. Sadowski, Lead shielding efficiency from the gamma background measurements in the salt cavern of the Polkowice–Sieroszowice copper mine. J Radioanal Nucl Chem 308 (2016) 773–780.

[31] L. Baudis, A.D. Ferella, A. Askin, J. Angle, E. Aprile, T. Bruch, A.Kish, M. Laubenstein, A. Manalaysay, T. Marrodán Undagoitia and M. Schumann, Gator: a low-background counting facility at

669 the Gran Sasso Underground Laboratory. Journal of Instrumentation, Volume 6 (2011) P08010
670 arXiv:1103.2125.
671 [32] G. Luzon, J.M. Carmona, S. Cebrian, F. Iguaz, I.G. Irastorza, H. Gomez, J. Morales, A. Ortiz de
672 Solorzano, A. Rodriguez, J. Ruz, A. Tomas, J.A. Villar, Characterization of the Canfranc underground
673 laboratory: status and future plans in Proceedings of the Six International Workshop on the
674 Identification of Dark Matter, ed. M. Axenides, G. Fanourakis, J. Vergados (2006) 514-519.
675 [33] FOREGS, Geochemical atlas of Europe, electronic version, 2018,
676 http://weppi.gtk.fi/publ/foregsatlas/index.php.
677 [34] J.K. Osmond and J.B. Cowart, The theory and uses of natural uranium isotopic variations in
678 hydrology. At. Energy Rev 144 (1976) 621-679.
679 [35] J. N. Abdurashitov, V. N. Gavrin, V. L. Matushko, A. A. Shikhin, V. E. Yants, J. Peltoniemi, T.
680 Keränen, Measurement of Neutron Background at the Pyhäsalmi mine for CUPP Project, Finland
681 (2006) http://arxiv.org/abs/nucl-ex/0607024v1.
682 [36] H. Wulandari, J. Jochum, W. Rau, F. von Feilitzsch, Neutron flux at the Gran Sasso underground
683 laboratory revisited. Astroparticle Physics 22(3-4) (2004) 313-322.
684 [37] J.A. Formaggio, C.J. Martoff, Background to sensitive experiments underground, Annu. Rev.
685 Nucl. Part. Sci. 54 (2004) 361–412.
686 [38] A. Best, J. Goerres, M. Junker, K-L. Kratz, M. Laubenstein, A. Long, S. Nisi, K. Smith, M.
687 Wiescher, Low energy neutron background in deep underground laboratories. Nuclear Instruments and
688 Methods in Physics Research A, 812 (2016) 1–6.
689 [39] Z. Dębicki, K. Jędrzejczak, J. Kaczmarczyk, M. Kasztelan, R. Lewandowski, J. Olechowski, J.
690 Szabelski, M. Szeptycka, P. Tokarski, Neutron flux measurements in the Gran Sasso national
691 laboratory and in the Slanic Prahova Salt Mine. Nucl. Instrum. Methods Phys. Res. A, 910 (2018)
692 133–138.
693 [40] T. Florkowski, Natural production long-lived radionuclides in geological formations. Report No.
694 AIEA-R-5060-F. IAEA, Vienna 1991.
695 [41] E.V. Bugaev, A. Misaki, V.A. Naumov, T.S. Sinegovskaya, S.I. Sinegovsky, N. Takahashi,
696 Atmospheric muon flux at sea level, underground, and underwater. Physical Review D 58(5) (1998)
697 054001.
698 [42] V.A. Kudryavtsev, N.J.C. Spooner, J.E. McMillan, Simulations of muon-induced neutron flux at
699 large depths underground. Nucl. Instrum. Methods Phys. Res. A 505.3 (2003) 688–698.
700 [43] V.A. Kudryavtsev, L. Pandola, V. Tomasello, Neutron- and muon-induced background in
701 underground physics experiments. European Physical Journal 36(2) (2008) 171-180.
702 [44] P. Morciano, F. Cipressa, A. Porrazzo, G. Esposito, M.A. Tabocchinib, G. Cencia, Fruit Flies
703 Provide New Insights in Low-Radiation Background Biology at the INFN Underground Gran Sasso
704 National Laboratory (LNGS). Radiation Research 190 (2018) 217–225.

[45] D. Jordan, J.L. Tain, A. Algora, J. Agramunt, C. Domingo-Pardo, M.B. Gomez-Hornillos, C. Domingo, (2019). Corrigendum to 'Measurement of the neutron background at the Canfranc Underground Laboratory LSC'. Astropart. Phys. 118 (2020) 102372

[46] J.-P. Cheng, K.-J. Kang, J.-M. li, J. Li, Y.-J. Li, Q. Yue, Z. Zeng, Y.-H. Chen, S.-Y. Wu, X.-D. Ji, H.T. Wong, The China Jinping Underground Laboratory and its early science. Annual Review of Nuclear and Particle Science 67 (2017) 231-251.

[47] A. Stochioiu, S. Bercea, M. Sahagia, C. Ivan, I. Tudor, A. Celarel, The measurement of the natural radiation background in a salt mine. Rom. Journ. Phys. 56(5–6) (2011) 757–761.

[48] M. Budzanowski, B. Burgkhardt, P. Olko, W. Pessara, M.P.R. Waligórski, Long-term investigation on self-irradiation and sensitivity to cosmic rays of TL detector types TLD-200, TLD-700, MCP-N and new phosphate glass dosemeter. Radiat Prot Dosim 66(1-4) (1996) 135-138.

Highlights:

- Gamma ray dose of 158±29 pSv/h was observed at the depth of 1436 m in felsic volcanic bedrock with sulphide deposit
- Deep underground location in pyrite mine has neutron flux of $(1.73 \pm 0.10)\times10^{-5}$ $cm^{-2}s^{-1}$
- Disequilibrium between ^{238}U and ^{226}Ra indicates the content of industrial wastes in wall coverage materials
- Increased intensity of gamma rays gives high-energy summation peaks on the spectrum
- Metal component susceptible on neutron activation are ^{24}Na, ^{28}Al, ^{46}Sc, ^{56}Mn, ^{59}Fe

Reply to Reviewer's comments
to the paper "Natural background radiation at Lab 2 of Callio Lab, Pyhäsalmi mine in Finland"

Dear Reviewers,

Thank you very much for your notes and all your help to correct and improve our paper. Below, we present a reply to your remarks.

Reviewer #1

1. Abstract: Specify that the neutron flux given here regards thermal neutrons.
Reply: The specification of „thermal" neutron flux was added in lines 38 and 40, to clarify the statement about measured component of neutron flux.

2. Line 49-50: "ensure a ", also possibly you want to replace "required for" with "as well as for".
Reply: "Ensure a low background" was the statement we wanted to give. This was corrected.

3. Line 51: "and the level"
Reply: This was corrected according to the Reviewer's suggestion.

4. Line 56-58: Cosmic muons are cosmic rays
Reply: Indeed, the cosmic muons are the cosmic rays, but to emphasize that, we corrected the statement in lines 56-58 by adding "(including muon)" and by removing "cosmic muon interactions"

5. Line 61: What do the authors want to say with "non-radioactive hazards"?
Reply: This was an editor's mistake. It should be "radioactive hazard" and it was corrected.

6. Line 119: "the neutron capture results [..]: -> "neutron capture on these elements does not result in the production of a radionuclide"
Reply: This part of a sentence was corrected according to the Reviewer's suggestion.

7. Line 154: It might be better to state the rock and water sampled were analysed in an outside laboratory using alpha and gamma spectrometry
Reply: The sentence about measurement techniques used was corrected, taking into account the Reviewer's suggestion.

8. Line 222: Shouldn't the series not already have been in equilibrium in the underground? And why should one month of storage help in the case equilibrium had somehow not previously been reached?
Reply: Rock samples isolated from external factors, only after a certain, sufficient time depending on half lives of analyzed radionuclides, may reach secular radioactive equilibrium. For measurement purposes sample is dried, crushed and homogenized, which could disturb the equilibrium between consecutive radionuclides in the decay chains. The gamma spectrometry measurements were carried out in a polyethylene containers. Therefore, samples were sealed to prevent the escape of ^{222}Rn and left for a month in order to obtain radioactive equilibrium between ^{226}Ra and its short lived daughters (1 month is sufficient in this case) as well as for isotopes present in ^{232}Th chain. This enables the analysis of ^{232}Th and ^{226}Ra on the base of their decay products. Such procedure was applied because ^{226}Ra gamma line is not convenient for analysis due to significant interference of ^{235}U (57.5 % emission probability) on the 186 keV gamma line of ^{226}Ra.

9. Line 232: Samples were spiked for what purpose?
Reply: At the beginning of the chemical analysis the ^{232}U isotope of a well-known activity was added to samples in order to quantify chemical recovery as well as ^{234,238}U concentrations, since the chemical efficiency may differ significantly from sample to sample. Using ^{232}U as a radiochemical tracer for

analysis of $^{234,238}U$ isotopes concentration is an established method for determination uranium content in water samples.

10: Line 253: "The neutron detection [..]" (the listing of missing articles by me is not exhaustive)
Reply: this was corrected and the entire text was reviewed for language corrections.

11. Line 262: The detectors appear to be the same as previously, maybe the electronics were upgraded?
Reply: The Reviewer was right, only the electronics was upgraded not the helium counters themselves. Therefore the statement "detectors themselves were upgraded" was replaced by "electronics was upgraded" not to confuse a reader.

12. Line 280: Presumably the stated alpha count rate is per counter; what alpha activity per surface of the counter material does that translate to?
Reply: Indeed, we presented the alpha count rate per counter. If it is assumed that alpha particles come from a steel tube of the counter, the count rate can be translated into surface activity equal 2.3 $\mu Bq/cm^2$. On the other hand, alpha particles might also come from a ceramic insulator between the tube and wire (anode). In this case, insulator surface activity would be much higher, but it is more difficult to assess. At present, it cannot be decided which origin is more probable.

13. Line 282: By "signal cut-off" you mean "pulse-shape analysis"?
Reply: The Reviewer was right. This was corrected.

14. Line 284-285: Has the pulse-shape analysis been tested on the surface/with a neutron source? What is the rejection rate for neutrons (false negatives)? The spectrum shown in Fig 3b looks rather messy (before PSA), a 2D histogram showing the exclusion and inclusion regions for the PSA would be helpful in convincing the reader that the method is under control.
Reply: The choice of neutrons using PSD is based on the differences in the rise time of signals from different particles. Since our ADC samples the signal quite rarely (every 1 μs), a good measure of the rise time is the maximum signal jump between two successive samples (on the rising edge of the signal). The attached drawing (also inserted in the text – Fig. 3b) shows a two dimensional histogram amplitude vs. maximum signal jump for one of the counters used during the measurements described in this paper. The neutrons are in the area "ACCEPTED", i.e. below the C1 line and above the C2 line. Points for neutrons form a triangle shaped ribbon with a vertical band at 115 ADC. This band corresponds to a full energy peak (764 keV). This shape of the distribution is probably related to the fact that the reaction products $^3He(n,p)^3H$ are moving in various directions relative to the counter wire (anode). Cases located in the same area but with amplitudes greater than 115 ADC are derived from alpha particles. Around the amplitude of 130 ADC a vertical band is visible associated with the saturation of the analog amplifier. Above the C1 line there are cases with a very short rise time. They probably come from high voltage leakage on insulators. Below the C2 line there are signals with low amplitudes and rise times greater than for neutrons. They probably originate from other ionizing particles. The C1 and C2 lines alone show the cuts used to select neutrons. Since the rejection of neutrons with the lowest amplitudes is not critical to the result (see below), the C2 cut is shifted slightly up.

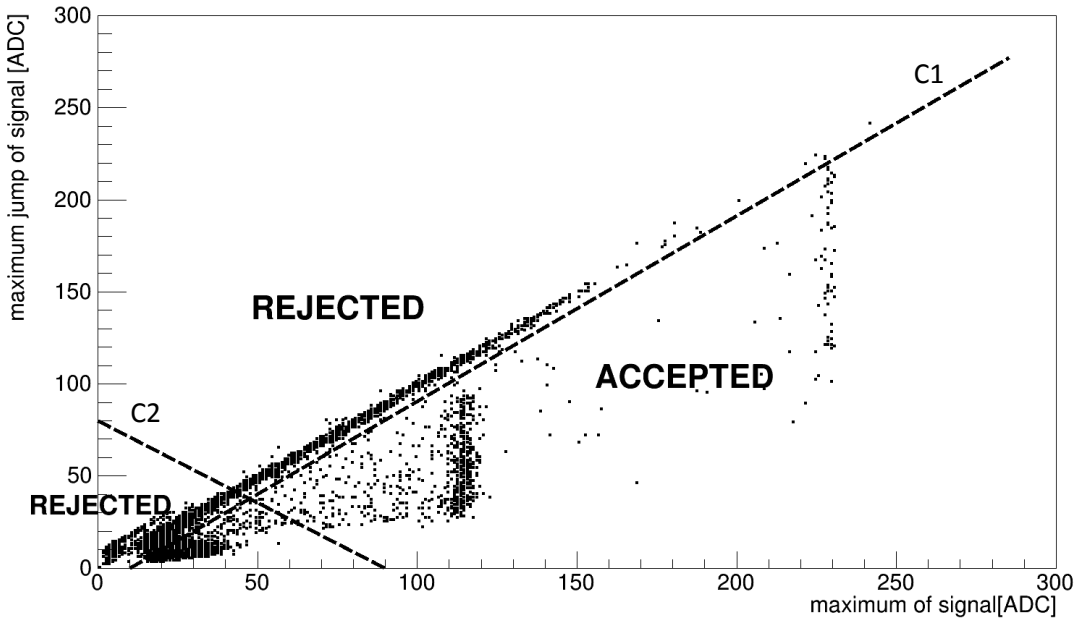

For accepted events, the spectrum of maximum values from the waveform was built up. An example of such a spectrum is shown in this article in the figure 3b (solid line) (now: fig. 3c). The characteristic structure of the helium counter spectrum is clearly visible: a 764 keV peak around 115 ADC and a tail of the wall effect reaching up to around 50 ADC. In this case the wall effect should reach to about 28 ADC, but part of the spectrum is rejected by cuts. However, the missing part can be determined by fitting the recorded part of the wall effect spectrum with a linear function and extending it to the expected end of the spectrum. By comparing the number of registered and missing events, one can determine the correction factor related to the cuts. Then, for the events accepted by the cuts, a distribution of count over time was made (for example see fig. 5a in this paper). This distribution is flat, so one can fit it with a linear function and this fit determines the counting rate. The value obtained must still be multiplied by the correction factor.

This procedure was used separately for each counter of the setup, and the results are shown in the table below. The order of the counters in the table corresponds to the position of the counter in the tray. One of the counters (No. 3) failed during the measurement, therefore it is not included in the analysis. The errors shown in the table are the result of the uncertainty of fitting linear functions to the distributions of count over time. The average of the results for individual counters was used as the final result. The error is a standard deviation from this average.

Counter number	Neutron count rate per 1 hour	Neutron flux $\times 10^{-5}$ [$cm^{-2}s^{-1}$]
1	13.9 ± 0.5	1.62 ± 0.06
2	14.8 ± 0.5	1.73 ± 0.06
3	breakdown	—
4	14.4 ± 0.5	1.68 ± 0.06
5	14.8 ± 0.5	1.73 ± 0.06
6	14.5 ± 0.5	1.70 ± 0.06
7	15.4 ± 0.6	1.80 ± 0.06
8	14.4 ± 0.5	1.68 ± 0.06
9	14.0 ± 0.5	1.64 ± 0.06
10	16.8 ± 0.6	1.96 ± 0.08

The assessment of the quality of cuts is difficult because during testing with neutron source (even very weak) the signal from neutrons dominates completely over all types of background. However, in the region of the full energy peak (764 keV) signal and background separation is close to 100%. Probably a much larger error in the assessment of the neutron flux is due to the simplifications in the simulation of the measurement setup environment. In test measurements under controlled

conditions (graphite well with counters and known weak source of neutrons) we obtain the agreement of measurement and simulation at the level of few percent.

15. Line 306-307: Over what time period does the radon concentration vary? Randomly in time or following a pattern?
Reply: The statement concerns the variation of radon concentration from one measurement point to another, since each of a gamma spectrometry measurement was accompanied by the measurement of radon concentration. The information about the period of time (24 h) of each radon measurement was added and the results were presented in more details.

16. Line 328-337: It is not clear how meaningful the count per second values are, as those depend on the detector used, thus are very hard to compare to measurements from other labs. The photon flux seems to be the only parameter that makes much sense here. Also, I assume the "photon flux density" refers to only the individual full-energy peaks? If so, also that value depends strongly on the detector.
Reply: The Reviewer was right, the cps values depend on the detector used, but it could be compared with other published data when the information about the detection efficiency is given and knowing that this is a commercially available equipment, i.e. not specially designed low-background setup. Since in other publications the information about the integral count rate is given, we decided to give such information to enable the comparison, even if it is rather rough. the photon flux density was assessed on the base of full-energy peaks but it takes into account the detector efficiency. Therefore, it seems to be not much dependent on the detector itself. The information about the assessment on the base of a full-energy peaks was added.

17. Table 2: The number of significant digits is excessive in many cases here.
Reply: Data in Table 2 have been changed from effective dose for each line to counts per second and the effective dose for each radionuclide was also given. We think that this make the results presented in Fig. 4 more complete, and basically there is no need to present the contribution to the effective dose from particular gamma line whereas the contribution from each radionuclide could be essential for the estimation of radiation hazard. Such changes were suggested by the other Reviewer. As for the presentation of the results, we would like to stay them consistent with the previous data [18], therefore they are presented with three decimal places.

18. Line 362: In reality the numbers here are all upper limits and should probably be stated as such
Reply: These values are simply the average over numbers presented in table 3. Therefore the standard deviation is so large. These SD values were intended to demonstrate the large differences in activity concentration from sample to sample. In this paragraph the reader could compare the data presented in table 3 in terms average value (which is of a minor importance due to large SD) with numbers provided by FOREGS.

19. Table 3: It appears that most of the locations (sample column) are not explained in the text.
Reply: The locations of samples collection were described in the text of subsection 2.2.

20. Line 433-435: State the detection efficiency coming from the simulation.
Reply: The explicit statement about the detection efficiency coming from the simulations was added.

21. Line 441: Is the statistical uncertainty included in the neutron flux value?
Reply: The average of the results for individual counters was used as the final result. The final uncertainty is then a standard deviation from the average. The statistical uncertainty for a single counter is one order of magnitude smaller, as shown in table where the fluxes of neutrons are presented (see: remark 14.)

Reviewer #2

ABSTRACT

1.38: I would write better "radon concentration determination".
Reply: This was corrected according to the Reviewer's suggestion.

1.41: it would be interesting to report also the final results for the flux of gamma rays and radon concentration.
Reply: The information regarding photon flux and radon concentration was added in the abstract.

INTRODUCTION
2.49: You could add to Refs. [1-4] some more recent references on underground labs like these ones:
- The world deep underground laboratories, A. Bettini, Eur. Phys. J. Plus (2012) 127: 114
- Review of technical features in underground laboratories, A. Ianni, International Journal of Modern Physics A Vol. 32 (2017) 1743001
Reply: According to the Reviewer's suggestion, the more recent references were added.

2.56: If the sentence refers to ULs, I would remove "cosmic ray interactions", as later specifically "cosmic muon interactions" are mentioned and no other cosmic rays arrive deep underground.
Reply: The sentence was reformulated to include muon interactions in a broad category of cosmic rays, since this statement describes the background generally, shallowly and deeply located.
Now it is as follows: "The known main sources of background radiation are: cosmic ray (including muon) interactions, the decays of primordial radionuclides (mainly ^{40}K, ^{232}Th, and ^{238}U), the neutron interactions that originate from (α,n) reactions, the spontaneous fission of U and Th."

2.65: again better "radon concentration determination"
Reply: The statement was corrected according to the Reviewer's suggestion.

2.65-68: later in section 4, muon flux measurements available are discussed. I guess muon measurements have not been made now because this background was fully characterized before. A mention to this could be done here.
Reply: According to the Reviewer's suggestion, the following sentence was added: "The muon flux measurements have not been performed, since the muon component was fully characterised earlier [8]."

Section 1.1: many geological details are given, which is really hard to follow for a physicist. Are all they relevant for the background measurements presented? If not, I suggest simplifying this section, highlighting the information useful for the interpretation of the background measurements.
Reply: This section was rewritten to give the information more relevant for physicists and the attention has been paid to the information about radioactive content of the rocks.

Indeed, I recommend you to consider to create a new section, with the contents of section 1.1 and the first two paragraphs of section 2, to present the laboratory including the geological information.
Reply: The two first paragraphs of section 2 were moved to the subsection 1.1, since they indeed provide the characterization of the site.

2.77: what is the meaning of NW in NW-trending? North-West?
Reply: The section was rewritten and now the shortcuts do not appear.

3.82 and 3.84: what is the meaning of a in the Ga units? (G, M I guess correspond to Giga, Mega).
Reply: The section was rewritten and now the shortcut does not appear.

3.91: the indicated contents of the mined ore do not sum 100%, which are the dominant elements not given?
Reply: Indeed, the indicated contents of the mined ore does not sum up to 100%. However, it is the standard convention that geochemical data of an ore are reported this way. By definition, the term "ore" means that the components that are part of the ore (i.e., they constitute it) must be economically viable for extraction (if not, the stuff is not ore). What is not an ore deposit now may be ore in the next

year, and so worth. Hence, when the contents of an ore are listed, only the components that are economically important at the time of writing are mentioned. In this case the sentence "Regarding valuable metals, the ore contain on average 0.92% Cu, 2.45% Zn, 37.4% S, 0.4 g/t Au and 14 g/t Ag" list those components of the ore that are important from the point of view of the mining operation (in this case for the Pyhäsalmi mine).
Nearly all rock pieces larger than a small pebble contain practically most elements from a periodic table. It is just a question of how much there is each element. If there is a reason to show the whole content of the rock, then geologists always use numeric tables, but it seems to be pointless in this paper. However, even then the sum of the components does not ever reach 100%, unless they are normalized mathematically to this (which is not often done). The reason for this is that many rocks contain so called volatile components that escape the rock before the analysis or they cannot be analyzed with the used method.

Table 1: for the mineral contents of sulphide ore, it is indicated "main mineral" and "accesory mineral", what are the criteria to fix it as main or accessory? If this information is not given for the other rocks presented in the table, I would not include it neither in this case.
Reply: Rocks are composed of minerals. From a geological point of view, a mineral is a naturally occurring substance which is usually solid, crystalline, stable at room temperature and inorganic. There are almost 5000 known mineral species, yet the vast majority of rocks are formed from combinations of a few common minerals, referred to as “rock-forming minerals”. The rock-forming minerals are: feldspars, quartz, amphiboles, micas, olivine, garnet, calcite, pyroxenes. In the case of ores (which are a special type of rocks), the term "rock-forming mineral" is changed to the term "main mineral". The definition is still the same, i.e., a main mineral is one of the major constitutes of the ore. Minerals occurring within a rock in small quantities are referred to as “accessory minerals”. The accessory minerals do not greatly affect the bulk composition of the rock. However, although accessory minerals are present in only small amounts, they may provide valuable insight into the geological history of a rock, and are often used to ascertain the age of a rock. In some ore deposits, like in Pyhäsalmi, the ore is so rich in ore minerals that they are main minerals themselves (like pyrite in Pyhäsalmi). Accessory minerals can be further subdivided into "main accessory minerals" (or "important accessory minerals") and "minor accessory minerals". The difference is typically not exactly defined.
Therefore, we would like to leave it like it was since the information presented in this table could be useful also for geologists and industry for whom these terms might be more meaningful and useful and from a physicists point of view they are not misleading.

4.124: Which is the difference between the elements reported here and those given before in line 114?
Reply: The elements mentioned in the line 114 are the main building materials, whereas the elements mentioned later are the admixtures in the rocks. Since the antimony was mentioned in the line 114, it was removed from the later statement.

MATERIALS AND METHODS
5.128: Section could be better titled as "Equipment and methods".
Reply: According to the reviewer’s suggestion, the title of this section was changed.

Figure 1: the depths indicated in the layout for labs 1 and 2 can hardly be read. It would be useful to indicate also those for labs 3 and 4.
Reply: The information about the location of the labs was added to the figure 1 caption.

6.148: Although Ref. [11] is given, you could briefly indicate here how the reported activities were obtained.
Reply: The activities for shotcrete (Ra, K, Th) mentioned in the ref. [11] (now [14]) are from the shotcrete suppliers self-monitoring documents. The activity is required by the industry. The measurements were conducted by the laboratory of Finnish Nuclear Safety Authority, but in the industry document these were presented without errors. Such information was added in the text at the end of subsection 1.1.

6.154: All gamma measurements took 48 h? The duration of measurements could be presented better in the next subsections describing the measurements.
Reply: One measurement in MP1 took 48h and this information was added in the text. Other gamma measurements were shorter and took from 1 to 24 hours.

6.161: "i.e. is the ventilation dominant" is not clear to me, could you explain this better?
Reply: The sentence was reformulated.

7.170: You could complete the title as "In-situ gamma spectrometry"
Reply: The subsection title was completed according to the Reviewer's suggestion.

7.172: the meaning of HPGe has been previously defined, here you can use it directly.
Reply: The Reviewer was right and the sentence was corrected accordingly.

7.176: #8194 is the number of channels? If so, you could state it more clearly.
Reply: The information regarding the number of channels was changed to be clearer.

7.191: was taken -> were taken
Reply: This mistake was corrected.

8.212: 3th -> 3^{rd}
Reply: This mistake was corrected.

8.221: remove "a" before polyethylene containers
Reply: This has been done.

8.228: gamma emission from ^{212}Pb is at 238.6 keV (not 338.6).
Reply: This mistake was corrected.

Do you combine directly the two emissions from ^{232}Th? Equilibrium could be broken at ^{228}Th having a half-life of 1.91 y, so activity from ^{212}Pb could be firstly assigned to ^{228}Th.
Reply: The activity concentrations of ^{226}Ra and ^{232}Th isotopes were calculated as the weighted mean of the activities of their daughter isotopes assuming radioactive secular equilibrium (which is most likely due to 1-month storage of a sample material before the analysis). On the other hand, ^{40}K activity was calculated straight from a gamma (1460.8 keV) line originating from this isotope.
The isotopes ^{228}Ac and ^{212}Pb are widely used for analysis ^{232}Th concentration in rock/soil samples (for example: Uosif et at., 2015; Guidotti et al., 2015) and also provide the information about radioactivity equilibrium between ^{228}Ra (^{228}Ac) and ^{228}Th (^{212}Pb) isotopes. According to (Chiozzi, et al) ^{232}Th series may be considered in equilibrium in most geological environments and in rocks older than 10^6 years (Guidotti et al., 2015).

Guidotti, L., Carini, F., Rossi, R., Gatti, M., Roberto, Cenci, M., Beone, G.M., 2015. Gamma-spectrometric measurement of radioactivity in agricultural soils of the Lombardia region, northern Italy. Journal of Environmental Radioactivity 142, 36-44, https://doi.org/10.1016/j.jenvrad.2015.01.010

Chiozzi, P., Pasquale,V, Verdoya, M., 2002. Naturally occurring radioactivity at the Alps–Apennines transition. Radiation Measurements 35 (2),147-154, https://doi.org/10.1016/S1350-4487(01)00288-8

Uosif, M.A.M.,Issa, S.A.M, Abd El-Salam, L.M., 2015. Measurement of natural radioactivity in granites and its quartz-bearing gold at El-Fawakhir area (Central Eastern Desert), Egypt. Journal of Radiation Research and Applied Sciences 8(3), 393-398, https://doi.org/10.1016/j.jrras.2015.02.005

You could give the energy of the gamma emission from ^{40}K with the same precision than others (one decimal place).
Reply: This has been corrected.

Section 2.2: MDA and counting times are given for the water samples. It would be useful to provide the same information also for the rock samples.
Reply: The information about MDA for rock sample analysis was added as follows: "Minimum detectable activity was equal to 0.4 mBq per sample for both ^{234,238}U isotopes."

Section 2.2: what about the samples of concrete wall mentioned before (page 6, line 156)? Are they included in the nine samples of rock described here? It seems so from tables 3-4, but it could be clarified here.
Reply: The locations of samples collection were clearer described in the text of subsection 2.2.

9.271-273: could you comment on the efficiency of the Pulse Shape Discrimination method applied to identify neutron events? I guess the filtering method is based on the signal cut-off described later in page 10, lines 282-285. As detectors are used to quantify a neutron flux, the effect of this efficiency is very relevant.
Reply: The choice of neutrons using PSD is based on the differences in the rise time of signals from different particles. Since our ADC samples the signal quite rarely (every 1 μs), a good measure of the rise time is the maximum signal jump between two successive samples (on the rising edge of the signal). The attached drawing (also inserted in the text – Fig. 3b) shows a two dimensional histogram amplitude vs. maximum signal jump for one of the counters used during the measurements described in this paper. The neutrons are in the area "ACCEPTED", i.e. below the C1 line and above the C2 line. Points for neutrons form a triangle shaped ribbon with a vertical band at 115 ADC. This band corresponds to a full energy peak (764 keV). This shape of the distribution is probably related to the fact that the reaction products $^{3}He(n,p)^{3}H$ are moving in various directions relative to the counter wire (anode). Cases located in the same area but with amplitudes greater than 115 ADC are derived from alpha particles. Around the amplitude of 130 ADC a vertical band is visible associated with the saturation of the analog amplifier. Above the C1 line there are cases with a very short rise time. They probably come from high voltage leakage on insulators. Below the C2 line there are signals with low amplitudes and rise times greater than for neutrons. They probably originate from other ionizing particles. The C1 and C2 lines alone show the cuts used to select neutrons. Since the rejection of neutrons with the lowest amplitudes is not critical to the result (see below), the C2 cut is shifted slightly up.

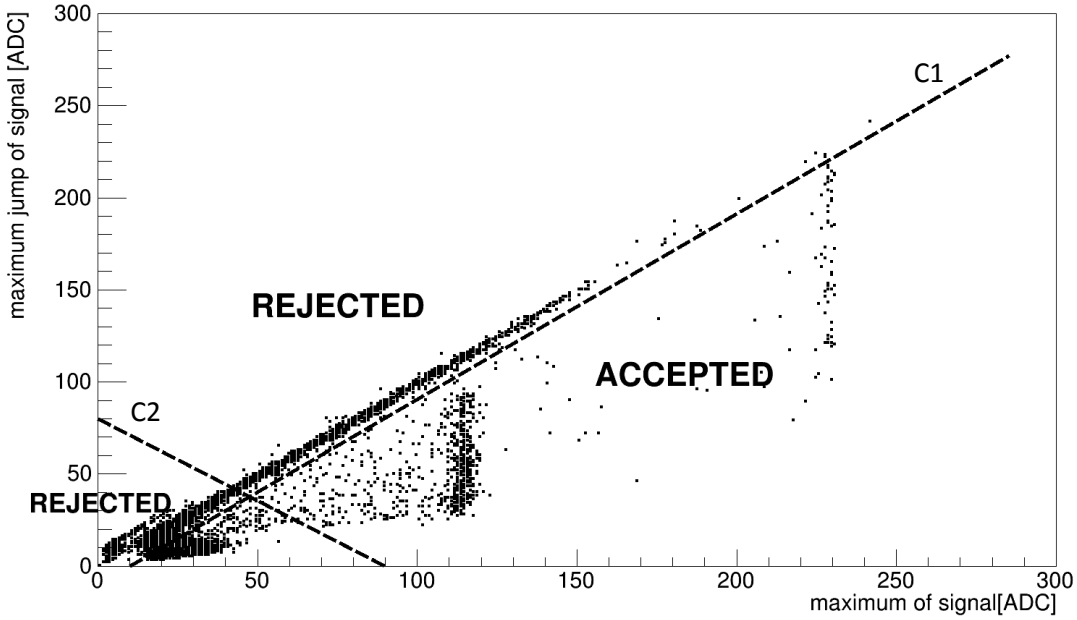

For accepted events, the spectrum of maximum values from the waveform was built up (fig. 3b – now fig. 3c).

10.280-282: could you comment on the origin (maybe internal background of the detector?) and the signal of the alpha events?
Reply: Alpha-emitters are the internal impurities of materials the counter is made of. Since alpha particles are emitted from various depths of counter body, they reach an active area of the counter having various energies, from nearly 0 to about 9 MeV (maximal energy of alpha particles emitted by the natural decay chains). Therefore they are recorded by the counter (using low gain measurements) as a flat rectangular spectrum extending in this energy range. This shape of the spectrum suggests that alpha particles are originally monoenergetic, but they are born at a random depth in some material, so they lose some of their energy before they reach the counter active volume. Therefore the spectrum is recorded as rectangular. If it is assumed that alpha particles come from a steel tube of the counter, the count rate can be translated into surface activity equal to 2.3 $\mu Bq/cm^2$. Another possibility is that the alpha particles come from a ceramic insulator between the tube and wire (anode). In this case, insulator surface activity must be much higher. At present, it cannot be decided which origin of alpha particles is more probable.
To be more informative, in the text a statement "from internal impurities of the counter body" was added" in relation to the alpha particles observed on ADC spectrum.

10.286: could you precise how neutron events are extracted from the spectrum of signal maximum amplitudes? I guess you select events of the peak around 115 ADC, but how exactly? As I pointed out before, as detectors are used to quantify a neutron flux, the efficiency of this selection is also very relevant. How "wall effect" is taken into account to determine the counting rate of neutron events?
Reply: The characteristic structure of the helium counter spectrum is the following: a 764 keV peak around 115 ADC and a tail of the wall effect reaching up to around 50 ADC. In this case the wall effect should reach to about 28 ADC, but part of the spectrum is rejected by cuts. However, the missing part can be determined by fitting the recorded part of the wall effect spectrum with a linear function and extending it to the expected end of the spectrum. By comparing the number of registered and missing events, one can determine the correction factor related to the cuts. Then, for the events accepted by the cuts, a distribution of count over time was made (for example see fig. 5a in this paper). This distribution is flat, so one can fit it with a linear function and this fit determines the counting rate. The value obtained must still be multiplied by the correction factor.

RESULTS
10.306-307: the indicated variation in radon concentration refers to variation in time or to variation at different measuring points? It is not stated if RAD7 detector was taking data during the 48 h of data taking for the HPGe detector, this could be clarified. As radon concentration can significantly change in time, the time span of the radon measurements is relevant. If measurements are available for the three MP, it would be very useful to present them clearly.
Reply: The results on radon concentration monitoring was presented in more details, as the Reviewer suggested.

10.307: it seems a bit strange to report the uncertainty as +-10%. You must indicate in any case how this 10 or 11% has been estimated, is it given by the detector specifications?
Reply: The concentrations are presented with two-sigma statistical uncertainty. According to the Detector User Manual (Rad7, Electronic Radon Detector User Manual, https://durridge.com/support/product-manuals/) RAD7 defines sigma as 1 + SQR(N+1), where N is the number of counts. The information about the concentration uncertainty was inserted in the text.

Figure 4: as the spectrum is an energy distribution, units for Y-axis must indicate the energy bin considered for plotting, that is, for example counts per second and per keV.
Reply: The presentation of the spectrum in Fig. 4 was corrected and now the Y-axis includes the information about energy binning.

Section 3.1: you present total effective dose at three measuring points (MP1-MP3) (lines 347-348); for the sake of completeness and for comparison, it would be very useful to show also the previous results

from gamma measurements at these other points MP2 and MP3, including the energy spectrum (as shown in Figure 1 for MP1) and the photon fluxes.
Reply: In our opinion there is no need to present the gamma energy spectra from points MP2 and MP3 as they are very similar to that collected in MP1 (no other gamma lines were observed in these points). However, for comparison purposes it might be useful to present photon fluxes, as the Reviewer suggested, and it was done. Qualitatively the spectra obtained in these tree points are the same and only counts in particular lines (and spectrum continuum position) are a little bit different, what is suggested by the differences in photon fluxes.

11.326-328: I suggest presenting the count rates at each line in a table and identifying the lines as in figure 4 and other parts of the text (one decimal). I guess statistical uncertainty in the rates is very small, but it can be quoted in any case. If possible, you could give the rates at the three MP.
Reply: According to the Reviewer's suggestion, counts per second were shown for each gamma lines (in Table 2). For comparison purposes, integral count rates up to 2700 keV from spectra measured in MP2 and MP3 were also presented. Data in MP2 and MP3 are only supportive to show there are no big differences between measuring points located nearer and further the wall of Hall 2, therefore they were not presented in such details as in MP1, which is the main experimental location in which also neutron flux was characterized. As for the presentation of the results, we would like to stay them consistent with the previous data [18], therefore they are presented with three decimal places.

12.331: the integral count rate could also be presented in the same new table. The reported uncertainty seems quite large (4%), is that OK? How has it been estimated? If correct, I would rather write 654+-26 (two significative digits for the uncertainty).
Reply: The information about integral count rates in all three measurement points was inserted in the text, since it has been estimated only up to 2700 keV to enable the comparison with other published data mostly restricted to that energy. The data was presented with two significant digits, as the Reviewer suggested. The uncertainty is simply the square root of integral count rate. Since the detector used is not made of low-background materials, the value of 4% is adequate.

12.335: it would be interesting to compare also the photon flux with those measured at other labs. Using for instance the reference I proposed in a previous comment (The world deep underground laboratories, A. Bettini, Eur. Phys. J. Plus (2012) 127: 114), the flux is around one order of magnitude higher than other labs.
Reply: The comparison of photon flux with data reported for several underground labs was added in the subsection 3.1.

12.335-337: how this other rate (total spectrum continuum) has been determined? This is not described in section 2.1.
Reply: The photon flux density was assessed on the base of a full-energy peaks, and the total spectrum continuum was estimated as a difference between the whole registered spectrum and all full-energy peaks. That explanation was added in the text of subsection 3.1.

12.341: I would express the activity giving two (three at most) significative digits for the uncertainty, that is, 59+-17 Bq/cm^2.
Reply: This was corrected according to the Reviewer's suggestion.

Table 2: I guess you decided to present all the results using three decimals, but I think it is more adequate to indicate all the results with the same precision giving for instance two significative digits for the uncertainty.
Reply: As stated above, we would like to stay them consistent with the previous data [18], therefore they are presented with three decimal places.

I consider it is not very useful to show the effective dose for each individual line (as other previous results like the gamma counting rate are not shown at such level of detail), it would be enough to show the total effective dose for each isotope.

Reply: The Reviewer was right, data in Table 2 have been changed from effective dose to counts per second for each gamma line and total effective dose for each isotope is also presented as more adequate information about radiation hazard.

14.357: I would use here the same notation used later in the paragraph (for an easier comparison of results), indicating mg/kg as ppm. I suggest also giving the natural potassium concentration rather than the percentage of K_2O.
Reply: This was corrected according to the Reviewer's suggestion.

14.362: I think the mean value should be for ^{226}Ra (not ^{238}U). The upper part of the chain has not been analyzed (due to low intensity of gamma emissions)? If possible, it would be interesting to make an estimate of ^{238}U activity to cross-check with alpha measurements.
Reply: It was corrected (^{238}U -> ^{226}Ra) as suggested by the Reviewer. The upper part of the decay chain has not been analyzed indeed, but the ^{238}U concentration might be estimated based on the measurement of ^{234}Th gamma line. However, it was not the subject of present study to compare results obtained from different nuclear spectrometry techniques.

14.362-363: does the given percentage correspond to ^{40}K? I recommend to present directly the corresponding activity (Bq/kg) as made for ^{238}U and ^{232}Th.
Reply: The presentation of ^{40}K content was changed from percentage to Bq/kg, according to the Reviewer's suggestion

14.363-364: concentrations from [11] give activities which are in the range defined taking into account the very large SD in the measurements presented here; uncertainty of SD are not reported in [11]?.
Reply: Very large SD for the presented concentrations are the result of big differences among values obtained from each samples as presented in Table 3. We decided to present it like this to pay attention to a very large variation of result which one might obtained taking the samples at a relatively small area. By the statement: "Therefore, the average values stated for the whole mine of 0.8 ppm U and 3.2 ppm Th [11] are not applicable here" we wanted to stress that since the differences are large, the average value reported in [11] (now [14]) should not be used to predict radiation conditions in studied localization of Pyhasalmi mine. That was also clarified in the text.
The uncertainties of concentration values given from [11] (now [14]) were added.

Table 3: I would change "Radioisotopes concentrations" to "Radioisotopes activity concentrations" in caption and "Radioactivity concentration" to "Activity concentration" in the columns.
Reply: This was corrected according to the Reviewer's suggestion.

Table 4 and 5: again, I would change "radioactivity concentration" to "activity concentration".
Reply: This was corrected according to the Reviewer's suggestion.

Table 3-4: Identification of some samples (PH_*, R-2229*) is obscure, could you indicate more clearly the origin, as for other samples?
Reply: The locations of samples collection were better described in the text of subsection 2.2.

15.386: I guess both gamma and alpha spectrometry have been used to derive the results in Table 5. It could be stated, as done in previous tables for rock samples.
Reply: As stated in subsection 2.2, results presented in Table 5 were obtained using LSC counter and alpha-spectrometry technique. This information was added in the heading of Table 5.

Table 4: alpha spectrometry analysis cannot give results for ^{232}Th chain or for the lower part of the ^{238}U chain? It would be useful to cross-check results from gamma and alpha spectrometry.
Reply: Uranium ^{238}U content could be estimated based on ^{234}Th isotope content, which emits low energy 63.41 keV photons with low emission probability (3.83 %). Low emission probability involves long time of measurement which is particularly troublesome for low-radioactive environmental samples. Also self-absorption correction for low energy gamma line should be estimated. For this

purposes alpha spectrometry technique was used to determine $^{234,238}U$ isotope concentrations as the uncertainty of gamma spectrometry in this case could be much higher.

15.387-388 and Table 5: sometimes it appears "/L" in the units, but I think the proper notation is "/l".
Reply: To avoid confusion with "1" (the number one) we decided to use capital "L", to be consistent with the previous paper [17]. Therefore in Table 5 it was corrected to "^{228}Ra [Bq/L]" and in the entire text the notation "/L" is used.

Table 5: I think the samples in the last two rows correspond to MP1 and MP2. If so, you could use this notation already defined and used.
Reply: The points of samples collection do not correspond directly to the points where gamma spectra were registered, therefore the use of MP1 and MP2 notation in Table 5 would be misleading. For the clarity of presentation the description of points of water samples collection was added in subsection 2.2.

16.397: I suggest presenting section 3.3 (with results from in-situ gamma measurements) before section 3.2, to describe together all the obtained results from the gamma measurements in the lab.
Reply: This was corrected according to the Reviewer's suggestion

16.400 and 401: I suggest writing "..., respectively, ..."
Reply: The Reviewer was right – it was corrected accordingly.

16.412: I think you refer to the spectrum in figure 4; to make this clearer you could include in the sentence "... measured in Callio Lab 2 (MP1) and shown in Fig. 4 were ..."
Reply: The Reviewer was right – it was corrected accordingly.

16.418: the neutron flux of the ^{252}Cf source is given in n/cm^2, but which is the unit time (per second, per minute...)?
Reply: The flux is per second and this information was updated.

16.420: as also thorium has been determined, I would change "radium and potassium concentration" to "radioisotopes concentration".
Reply: The Reviewer was right – it was corrected accordingly.

17.424-425: it would be better to indicate the isotope for the two lines attributed to manganese and sodium.
Reply: It was corrected according to the Reviewer's suggestion.

17.434-435: I do not understand the last sentence about high concentration of selenium, as no selenium isotope is reported to have been identified after the irradiation of the rock samples.
Reply: By mistake "scandium" was changed to "selenium". This sentence applies to scandium and it has been corrected.

Section 3.4: it could be completed with an assessment of real danger of neutron activation from the environmental neutron flux in normal conditions.
Reply: The NAA measurements were design only as qualitative, i.e. sample was not specially prepared for taking into account self absorption of induced gammas as well as to maintain the uniformity of neutron flux through the entire sample. Moreover, no special attention was paid to the detection efficiency (geometry of the setup detector – sample) during spectrum registration. Therefore any quantitative assessment in terms of radiation hazard would be highly imprecise. The only estimation which is possible in this study, is to predict the maximal count rate in particular gamma lines assuming the activation during in-situ investigations occurs at the first few cm of the rock (self absorption is negligible). Such assessment was added in subsection 3.4 as the last paragraph. This was possible by scaling the counts per second in saturation conditions, where the scaling factor was the neutron flux. By saturation conditions we mean a state in which radioisotope activity does not increase

anymore and the processes of radionuclide activation and radioactive decay are in equilibrium. Such conditions are fulfilled when the neutron flux is constant over time and this could be assumed in environmental measurements like in presented study of Callio Lab.

17.432: as there are significant differences in the modeling of neutron interactions in different Geant4 versions, you could indicate the one you used.
Reply: The simulations were carried out using the Geant4 package version 10.04 with the physical package QGSP_BERT_HP and Neutron HP Thermal Scattering which are important for low-energy neutron interactions with nucleons bound in nuclei. We use this set as our standard neutron simulation kit, although in this particular case neutrons travel through the vacuum. In this simulation, the helium counter tray model was placed in the center of an empty sphere with a diameter of 3 m. Every point of this sphere was an isotropic source of thermal neutrons. This was done to ensure the neutron flux in the center of the sphere is isotropic. Then, the ratio of simulated counter response, i.e. neutron count rate, to simulated neutron flux was determined. Knowing this ratio and the measured count rate one can determine the neutron flux at the measurement site.
The information about the version of GEANT4 and physical packages was added to the text of subsection 3.5.

17.433-435: which has been the energy of the simulated neutrons (fixed or with some distribution over a particular range)? The estimated coefficient is the same for all the counters? It could be useful to report the obtained value and to indicate if uncertainty for it has been somehow quantified. I think it could be interesting to show in a table the neutron flux obtained for each counter (as in fig. 5.b numbers cannot be precisely deduced), even including also the counting rates, reporting the corresponding uncertainties if quantified.
Reply: Monoenergetic neutrons with energy equal to 0.024 eV were used in the simulation. One coefficient was used for all counters. The table containing the results of count rate and neutron flux for all helium counters was inserted in the text.

Figure 5: could you improve the quality of the plots? Legends are hardly readable. Plot a is just for one counter or for all? This could be clarified in the caption. The purpose of this plot a is to show stability over time? If so, this could be commented in the text. Range of X axis in plot b should be reduced, as values are concentrated in 15^{-20} 10^{-6} s^{-1} cm^{-2}.
Reply: The plot in fig. 5a is for a single helium counter and this was clarified in the caption. Also the comment of the stability of signal demonstrated in this figure was inserted in the text. The plot in fig. 5b was corrected. The quality of plots in fig. 3 and 5 was improved, as suggested by the Reviewer.

17.445-446: I do not understand the sentence "These energy ranges roughly correspond to the energies covered in the presented study" since the measured neutron flux gives the thermal component. I would suppress it.
Reply: This sentence was removed but the information was incorporated in the previous sentence as we think it is important.

DISCUSSION AND CONCLUSIONS
The discussion presented in this section is very interesting and includes background components not directly measured is this work (like the muon flux, neutron yields from radioactivity and muon-induced neutrons). But I think it should be included also a summary of the relevant results obtained from the measurements in the work: values of gamma flux, radon concentration, dose rate, activity in rock and water, neutron flux.
Reply: The paragraph briefly presenting the results was added in section 4, according to the Reviewer's suggestion.

18.467-472: Ref. [32] is given for U and Th concentrations in granite rock. Could you provide also some references for the quoted concentrations in the other types of rock?
Reply: The references were added in the text and the paragraph was slightly expanded.

19.487: remove "a" before "significant changes"
Reply: This was done according to the Reviewer's suggestion.

19.493: could you indicate the origin on the estimated uncertainty for the muon-induced neutron flux (from muon flux, from fitting function...)?
Reply: Muon-induced neutron flux was calculated from the equation given in ref. [5] (now [7]). This equation gives neutron flux as a function of one variable – depth in terms of water equivalent, and two fit parameters, which are given together with uncertainties. Therefore the uncertainty of neutron flux was calculated using total derivative method, however the depth was taken as an exact value without any error. The calculation was checked for consistency and slightly corrected. In the text a statement: "the uncertainty was calculated based on the uncertainties of fitting parameters presented in [7]" was added to clarified the origin of the presented uncertainty.

19.504-506: why the comparison to SNOLAB and SURF neutron flux is explicitly made, if values are also of the same order of magnitude than the one measured for Callio Lab 2, as for the other labs mentioned in Korea, China, Japan and Spain? I would just say that all the results are at the same level or show all the numbers. I think there is a mistake in line 504 when referencing with [39], corresponding to a study in Gran Sasso, the flux measured in SNOLAB.
Reply: We wanted to stress that results from labs located at shallower depths are closer to results obtained by us than data reported for labs located at a depths similar to Callio Lab 2. According to the Reviewer's suggestion, the sentence was corrected to avoid the confusion of the Reader.
The reference citing neutron flux for SNOLAB was corrected.

19.504: change For SNOLAB to for SNOLAB
Reply: This was done according to the Reviewer's suggestion.

19.505: change 0,8 to 0.8
Reply: Following the Reviewer's suggestion from remark 19.504-506, the sentence was reformulated and the value was removed.

19.508: I would give here just general references like [1,2], otherwise, you should quote most of the references of the paper, related to measurements of muon, neutron and gamma ray fluxes.
Reply: This was corrected according to the Reviewer's suggestion.

19.515-517: some doses are given in Gy, but it would make the comparison of results easier, to present all the results converted to Sv.
Reply: The Reviewer was right, the units should be unified for the purpose of a comparison. Since in all the cited references the dose type (air absorbed dose or dose equivalent) was clearly stated, it was possible to convert doses from Gy to Sv and this was done.

REFERENCES
1: You should include the published reference: AIP, Conf. Proc. 1338 (2011) 12.
Reply: This was done according to the Reviewer's suggestion.

6-8, 13: these references seem quite unclear to me. Are they reports, book chapters, or conference proceedings? Could you provide a more precise identification?
Reply: Ref. [13] (now [16]) is a report of the Swedish Radiation Protection Institute – this was more precisely described. Ref. [6] (now [9]) is a book chapter, which was more precisely presented, ref. [7] (now [10]) is a report, what was previously stated and now also link to the electronic version is provided, ref. [8] (now [11]) is a geological technical report and now also link to the electronic version is provided.

28: Page of the contribution is missing.
Reply: The page number was added.

40: Reference to the corrigendum can be simplified as it is already published at Astropart. Phys. 118 (2020) 102372.
Reply: This was corrected according to the Reviewer's suggestion.

41: You should include the published reference: Annual Review of Nuclear and Particle Science 67, 231-251 (2017).
Reply: This was corrected according to the Reviewer's suggestion.

***Credit Author Statement**

CRediT author statement

Kinga Polaczek-Grelik: Conceptualization, Methodology, Investigation, Writing - Original Draft

Agata Walencik-Łata: Methodology, Formal analysis, Investigation

Katarzyna Szkliniarz: Formal analysis, Writing - Original Draft

Jan Kisiel: Conceptualization, Methodology, Visualization, Supervision

Karol Jędrzejczak: Investigation, Writing - Original Draft

Jacek Szabelski: Investigation

Marcin Kasztelan: Formal analysis, Data Curation

Jerzy Orzechowski: Resources

Przemysław Tokarski: Resources

Włodzimierz Marszał: Resources

Marika Przybylak: Investigation

Jari Joutsenvaara: Conceptualization, Visualization, Project administration, Funding acquisition

Hannah J. Puputti: Investigation

Marko Holma: Writing - Original Draft

Timo Enqvist: Validation, Writing - Review & Editing

***Declaration of Interest Statement**

Declaration of interests

☒The authors declare that they have no known competing financial interests or personal relationships that could have appeared to influence the work reported in this paper.

☐The authors declare the following financial interests/personal relationships which may be considered as potential competing interests: